LAWRENCE
LIVERMORE
NATIONAL
LABORATORY

LLNL-CONF-860830

Frustraum 1100 Experimental Campaign on the National Ignition Facility

K. L. Baker, P. A. Amendt, D. A. Mariscal, H. Sio, O. L. Landen, D. D. Ho, V. A. Smalyuk, J. D. Lindl, J. S. Ross, N. Aybar, N. Birge, D. Casey, P. M. Celliers, H. Chen, D. Fittinghoff, H. Geppert-Kleinrath, V. Geppert-Kleinrath, S. Glenzer, S. W. Haan, D. Hinkel, S. Khan, A. Kritcher, M. Millot, J. L. Milovich, R. Nora, A. Pak, Y. Ping, J. Ralph, N. Roskopf, D. J. Strozzi, C. Young, B. Woodworth

February 24, 2024

The International Conference on Inertial Fusion Sciences and Applications
Denver, CO, United States
September 25, 2023 through September 29, 2023

Frustraum 1100 Experimental Campaign on the National Ignition Facility

K. L. Baker[1], P. A. Amendt[1], D. A. Mariscal[1], H. Sio[1], O. L. Landen[1], D. D. Ho[1], V. A. Smalyuk[1], J. D. Lindl[1], J. S. Ross[1], N. Aybar, N. W. Birge[2], D. T. Casey[1], P. M. Celliers[1], H. Chen[1], D. Fittinghoff[1], H. Geppert-Kleinrath[2], V. Geppert-Kleinrath[2], S. H. Glenzer[3], S. W. Haan[1], D. E. Hinkel[1], S. F. Khan[1], A. L. Kritcher[1], M. Millot[1], J. L. Milovich[1], R. C. Nora[1], A. Pak[1], Y. Ping[1], J. E. Ralph[1], N. Roskopf[1], M. S. Rubery[1], D. J. Strozzi[1], B. N. Woodworth[1] and C. V. Young[1]

[1]*Lawrence Livermore National Laboratory, Livermore, CA 94550, USA*

[2]*Los Alamos National Laboratory, Los Alamos NM 87544, USA*

[3]*Stanford University, Menlo Park, CA 94025, USA*

[a)]**Author to whom correspondence should be addressed:** baker7@llnl.gov

Abstract

We present findings from an experimental tuning campaign aimed at igniting larger DT cryogenic layered implosions using a dual frustum shaped hohlraum, denoted “frustraum”. The frustraum's distinctive shape reduces hohlraum wall losses while concurrently enhancing minimum capsule clearance with the hohlraum wall and sensitivity to pointing changes. Compared to current cylindrical hohlraum (6.4x11.3 mm), the frustraum has a wall area approximately 22% smaller, resulting in a measured improvement in efficiency of around 14%. Consequently, 14% less laser energy is required to implode a capsule within the same acceleration timeframe. Conversely, directing the same laser energy into the frustraum yields higher ion temperatures

within symmetry capsules, along with increased radiation temperatures and reduced implosion acceleration times compared to current cylindrical hohlraums.

I. INTRODUCTION

In indirect drive inertial confinement fusion (ICF) at the National Ignition Facility (NIF), a deuterium-tritium (DT) filled capsule[1, 2] is imploded by the ablation pressure generated by x-rays in a hohlraum with a peak radiation temperatures (T_r) of approximately 300 eV. These x-rays are produced by irradiating the interior of the high-Z hohlraum with 192 laser beams entering through two laser entrance holes (LEHs) positioned on either end. For the DT hotspot to initiate thermonuclear burn, it must attain high ion temperatures (T_{ion} >5 keV) and high hot spot areal densities (ρr_{hs} > 0.2–0.3 g/cm^2). The overall yield increases with confinement time, determined by the total areal density of the DT and remaining ablator, typically between 1–2 g/cm^2.

The objective of the National Ignition Facility (NIF) is to surpass the ignition threshold and maximize the released fusion energy in inertial confinement fusion (ICF) experiments, exceeding the input laser energy. We recently reported on layered implosions driven by a large frustraum, measuring 9.26 mm in diameter and 12.24 mm in length, employing High Density Carbon (HDC) capsules with an inner radius of 1.2 mm.[3, 4] This frustraum setup, illustrated in Figure 1, achieved the highest capsule absorbed energy attained on the NIF with laser energies below 2.05 MJ. Subsequent experiments utilizing 1.05 mm HDC capsules at 2.05 and 2.2 MJ surpassed the absorbed energy levels observed in the larger frustraum trials conducted at 1.7 MJ of laser energy (N210725). With the reduced laser energy of 1.7 MJ and the utilization of larger capsules, these experiments resulted in implosions with extended coast times, defined as the time between end of laser drive and bangtime, exceeding 1.8 ns. The prolonged coast times contributed to a decrease in radiation flux within the frustraum by the time of peak implosion velocity, as radiation drive in the hohlraum/frustraum diminishes exponentially once the laser is turned off.[3, 5] This diminished drive is correlated with the reduction in the down-scattered ratio (DSR) and compression in these implosions, as depicted in Fig. 2. Fig. 2a shows the measured DSR divided by the initial ice thickness and Fig. 2b shows the DSR with corrections for yield amplification, mode 1 and mode 2. The figures illustrate that for coast times in excess of approximately 1 ns, the maximum attainable compression diminishes exponentially with coast time across various HDC campaigns. As highlighted in our previous work[3], these reduced DSRs necessitate higher yields and ion temperatures to achieve ignition. Consequently, this motivated a transition to a smaller and more efficient frustraum, and a smaller 1.1 mm inner radius capsules (still later than the 1.05 mm used to demonstrate ignition), to mitigate coast time and lower the thresholds required for yield and ion temperature to achieve ignition. The data in Fig. 2 suggest, however, that for the SQN campaign with a shorter hohlraum cooling time than the frustraum and a smaller capsule, 0.91 vs. 1.1 mm I.R., that there is no apparent change in compression for coast times less than a nanosecond.[6, 7] With the increased laser energy now available on the NIF, at 2.2 MJ, larger frustraums and capsule sizes have become feasible for higher performance and larger-scale implosions.

The reduced wall area of the smaller frustraum enhances its efficiency compared to the current cylindrical hohlraum utilized on the NIF, leading to decreased losses. The power balance within a hohlraum can be succinctly expressed as shown in Eq. 1.[8, 9] The x-rays imploding the capsule within the hohlraum are produced by the laser power, P_L, entering the laser entrance holes and interacting with the wall. The level of x-rays produced is simply the laser power multiplied by the conversion factor of laser power into x rays, η. Losses to the hohlraum walls are expressed as the x-ray flux inside the hohlraum, σT_r^4, multiplied by the wall area, A_{wall}, and the factor $(1 - \alpha_{wall})$, representing the fraction of x-ray power lost to the walls where α_{wall} is the reemitted fraction or wall albedo. Likewise, power lost to the capsule is the x-ray flux within the hohlraum multiplied by the capsule's surface area, A_{cap}, and the absorption factor ($1-\alpha_{cap}$), where α_{cap} represents the capsule albedo. The x-ray power lost through the laser entrance holes is simply the x-ray flux inside the hohlraum, multiplied by the surface area of the laser entrance holes, A_{LEH}.

$$\eta P_L = \sigma T_r^4\left[\left(1-\alpha_{cap}\right)A_{cap} + (1-\alpha_{wall})A_{wall} + A_{LEH}\right]. \quad (1$$

The effective loss area of the hohlraum is then equal to $\left[\left(1-\alpha_{cap}\right)A_{cap} + (1-\alpha_{wall})A_{wall} + A_{LEH}\right]$.

The efficiency improvement between the two configurations can be quantified by comparing the ratio of their effective loss areas. The wall area of a cylindrical hohlraum A_{cyl}, with length L_{cyl}, main body radius R_{cyl}, curved ends of radius R_{end}, and LEH radius R_{LEH} is given by

$$A_{cyl} = 2\pi R_{cyl}\left(L_{cyl} - 2R_{cyl}\right) + 2\pi\left(\left(R_{cyl} - R_{end}\right)^2 - R_{LEH}^2\right) + 2\left(\pi^2 R_{cyl}R_{end} - \pi R_{cyl}^2(\pi-2)\right). \quad (2$$

The wall area of a frustraum hohlraum, A_{Fr}, with an equatorial radius, R_{eq}, radius at the LEH plane, R_{pole}, and walls at an angle θ is given by

$$A_{Fr} = \frac{2\pi\left(R_{eq}^2 - R_{pole}^2\right)}{sin(\theta)} + 2\pi\left(R_{pole}^2 - R_{LEH}^2\right) \quad (3$$

The reduced size frustraum, featuring a 25° wall angle, has a wall area of 2.05 cm², while the cylindrical hohlraum used for igniting capsules has a wall area of 2.57 cm². Consequently, the 1100 frustraum campaign reduces the wall area by approximately 22% compared to the HyE campaign and simultaneously increases capsule size by 5% to enhance coupling. With the same 3.1 mm laser entrance holes (LEH), the overall efficiency gain is estimated at around 14%, assuming a peak averaged wall albedo (α_{wall}) of 0.85.

In Section II, we describe the experimental parameters of the frustraum 1100 campaign. This campaign encompassed two frustraum geometries: the first measuring 7.8 mm in diameter at the capsule equator by 9.7 mm in length, with 23° wall angle, and the second measuring 8.2 mm in diameter at the capsule equator by 9.7 mm in length, with 25° wall angle. Section III presents the hotspot shapes observed in both campaigns and elucidates how this information guided our transition from the 7.8 mm frustraum to the 8.2 mm frustraum. In Section IV, we scrutinize the efficiency enhancements observed in the two frustraum scales, examining changes in acceleration time, ion temperature, and peak Dante flux relative to laser energy. Section V outlines the capsule intended for use in a layered implosion and presents 1D capsule-only simulation results comparing it to a HyE experiment. Finally, in Section VI, we summarize the findings of this frustraum platform and propose potential enhancements to bolster its future performance.

I. EXPERIMENTAL DETAILS

The experiments detailed in this article employed a frustraum geometry for the hohlraum configuration.[3, 4] Although two different frustraum geometries were utilized for these experiments, both incorporated laser entrance holes (LEH) measuring 3.1 mm in diameter at each end of the frustraum, and both employed 1.1 mm inner radius (I.R.) HDC capsules. Both frustraums measured 9.7 mm in length with R_{pole} = 1.84 mm, differing in wall angle (23° versus 25°), R_{eq} (7.8 vs 8.2 mm) and hence A_{wall} (1.95 vs 2.05 cm^2). For comparison, cylindrical hohlraums used in the HyE campaign measured 6.4 mm in diameter by 11.3 mm in length, with A_{wall} = 2.57 cm^2.

The hohlraums discussed in this article were constructed with gold walls. However, for future higher-energy shots, we plan to transition to more efficient, higher albedo gold-lined uranium walls. The HDC capsules positioned at the center of the frustraum had an inner radius of

1.1 mm and an overall shell thickness of approximately 77 µm. These capsules comprised a clean 6.7 µm-thick HDC layer on the inner shell, followed by a doped layer containing 0.35% tungsten (W) dopant 23.4 µm-thick, with the outer layer consisting of clean HDC material 47.4 µm-thick. In the symmetry tuning experiments detailed below, the capsules were primarily filled with deuterium at 1817 Torr or a mixture of 67%/33% D^3He at 2164 Torr, yielding an initial mass density inside the capsule of 4 mg/cm³ at the fielding temperature of 32° K. Additionally, all frustraums were filled with 0.3 mg/cm³ of ^4He gas also used in current cylindrical hohlraums. The implosions were driven by a three-stage laser pulse shape designed to generate three primary levels of x-ray drive in the hohlraum, thus exerting x-ray ablation pressure on the capsules and sending three primary shocks into the HDC ablator. These pulse shapes were modeled after the igniting HyE design.[10, 11]

A) THE 780 CAMPAIGN

The first frustraum 1100 campaign used the 23° wall angle version, as previously described, to drive the implosions. This campaign included an experiment aimed at measuring shock velocities and shock symmetry in the liquid deuterium in the interior of the HDC ablator utilizing a "keyhole" platform. Figure 3 illustrates a comparison of the measured shock velocities along the equator for the keyhole experiment, denoted as N220608, depicted as a dashed red line, juxtaposed with velocities from the HyE keyhole, labeled as N211031, represented by the dashed black line. Additionally, figure 3 includes the pulse shapes utilized to drive the experiments for the frustraum shot N220608 depicted as the solid red line and for the HyE N211031 shown as the solid black line. N220608 is able to achieve the same first shock velocity as the HyE N211031 with a 34% lower picket energy due to the increased efficiency of the frustraum 780 geometry relative to the cylindrical hohlraum used in N211031.

A gas-filled capsule implosion experiment denoted symcap (N220627) and an inflight x-ray radiography experiment denoted 2-D convergent ablator or 2D ConA, (N220523) were also conducted. The 2D ConA experiment employed a wavelength separation (at 1ω) of 0.8 Å and 0.1 Å between the inner and 50° cones and between the 45° and 50°, respectively. The later symcap experiment increased that to 1.4 Å and 0.4 Å given that the core shape was strongly oblate. N220523 utilized 1.4 MJ of laser energy into the frustraum, while N220627 employed 1.54 MJ of laser energy. Since the hotspots measured in the two experiments were both oblate, as depicted in Fig. 4a and 4b, it was decided to increase the wall angle of the frustraum from 23° to 25°, which by geometry moves the outer spots laser deposition region closer to the equator to drive the capsule more prolate. This had been already demonstrated in the larger-scale frustraum where transitioning from a 23° to a 25° wall angle resulted in implosions that were more prolate by approximately 45 μm.

This campaign also experimented with various quad splitting levels to assess their impact on the uniformity of wall illumination. Each quad, consisting of four beams, was split into two groups of two beams separated in azimuth, with each group containing two orthogonally polarized beams. This separation, known as quad splitting, was implemented to reduce wall intensity and mitigate stimulated Brillouin scattering. Figure 5 provides a view from the polar axis at 6 ns, looking through the laser entrance holes (LEH), illustrating three different quad splitting levels. Figure 5a shows no quad splitting, while Figure 5b features ±275 μm of quad splitting, and Figure 5c displays ±400 μm of quad splitting. Lineouts of the emission at 6 ns show that the 50% peak emission of the radial average occurs at 0.99 mm from the equator with no quad splitting(5a), 1.17 mm with ±275 μm quad splitting(5b) and 1.14 mm with ±400 μm quad splitting(5c). This indicates a reduced radial bubble velocity in the case of the ±275 and ±400 μm quad splitting relative to the case of no quad splitting,

B) THE 820 CAMPAIGN

The initial 780 frustraum campaign drove oblate implosions, prompting a redesign with 25° wall angles. Both designs maintain the same width in the LEH plane, leading to a slightly wider frustraum (8.2 mm) at the equator of the capsule for the 25° wall angle. This campaign also measured the shock velocities and symmetry. Figure 6 depicts a comparison of the measured shock velocities along the equator for the keyhole, N221005, represented by the dashed red line, with the velocities from the HyE keyhole, N211031, represented by the dashed black line. The pulse shapes used to drive the experiments are also shown, with the frustraum N221005 represented by the the solid red line and the HyE N211031 by the solid black line. N221005 is able to achieve the same first shock velocity as the HyE N211031 with a 19% lower picket energy due to the increased efficiency of the frustraum 820 geometry relative to the cylindrical hohlraum used in N211031.

A symcap (N221113) and 2D ConA experiment (N221220) were then conducted. The symcap experiment employed a wavelength separation (at 1ω) of 2.4 Å and 0.4 Å between the inner and 50° cone and between the 45° and 50°, respectively. Based on getting a prolate implosion, the later 2DConA experiment decreased the inner to outer cone Δλ to 1.25 Å. N221113 utilized 1.4 MJ of laser energy into the frustraum, while N221220 employed 1.6 MJ of laser energy. The hotspots observed in both experiments were prolate, as depicted in Fig. 7a and 7b, indicating that the wall angle change was successful in shifting the implosions in the intended prolate direction.

The 2D-ConA platform utilizes two quads of the laser, totaling 8 beams, to drive a backlighter foil, as illustrated in Figure. 8b. This setup enables the imploding capsule to be radiographed using a 9 keV zinc line emission backlighter. However, the backlit image in Fig. 8a revealed an x-pattern superimposed on top of the expected absorption features from the imploding capsule, thereby hindering the measurement of the inflight P4 of the imploding capsule. We hypothesize that this anomaly is caused by gold plasma flow collisions that emanate from just outside the corner regions of the diagnostic window cutout, as depicted in Fig. 8c. Notably, this phenomenon is not observed in singly curved cylindrical hohlraums or in the larger-scale frustraums where the drive duration was shorter. To validate this hypothesis, we intend to utilize a circular window in future 2D-ConA experiments as shown in Fig. 8d, to facilitate the measurement of both the inflight P2 and P4 of the imploding capsule.

II. CORE SHAPE CHANGES BETWEEN THE FRUSTRAUM 780 AND 820 PLATFORMS

The changes observed in the hotspot shape were consistent with measurements from larger-scale frustraum experiments.[3] In these larger-scale frustraums, a +45 μm change in the hotspot P2 was measured when the wall angle was increased from 23° to 25°. Additionally, a sensitivity to cross-beam energy transfer of approximately 40 μm/Å was measured for two colors applied between the inner and outer cones, at 1 ω. Figure 9 illustrates the hotspot shapes from three of the experiments. The hotspot from the 780 campaign experiment N220627 is depicted in the lower left of the plot. This experiment exhibited a very oblate shape with a P2 of approximately -55 μm, a two-color delta lambda of 1 Å, and a wall angle of 23°. The 2D-ConA experiment, N221220, in the middle of Fig. 9 was prolate with a P2 of approximately 14 μm, a two-color delta lambda of 1.25 Å, and a wall angle of 25°. The difference of ~69 μm in P2 between these two experiments is consistent with the expected 45 μm increase from transitioning from a wall angle of 23° to 25° and the expected 40 μm/4 = 10 μm increase from going from 1 Å to 1.25 Å, totaling ~55 μm. The additional increases in P2 arose due to the fact that N221220 was a 2D-ConA experiment in which two of the outer quads were removed to drive the backlighter foil. Similarly, the experiment in the top right of Fig. 9, N221113, had a two-color delta lambda of 2 Å relative to the 1.25 Å for N221220. The ~36 μm change between these two shots is primarily attributed to the expected 40 μm(3/4) = 30 μm increase in P2 in going from 1.25 Å to 2 Å of two-color between the inner and outer cones.

All symcap and 2D-ConA experiments can be incorporated into the empirical shape model developed for the larger-scale frustraum shots. In Fig. 10, the three experiments from the 780 campaign are depicted as green circles, while the two experiments from the 820 campaign are shown as red circles. The y-axis represents P2 at 33% cone fraction, while the x axis represents the expression $\mathrm{sqrt}(E_{out}/A/\rho)^{0.5}(\tau/R_{hohl})^{2}(CCR)^{0.5}$, as illustrated in Fig. 10. Here E_{out} is the energy in the picket of the outer beams, A is the area of the outer beams, ρ is the density of the hohlraum gas, and τ is the time between the beginning and the middle of the peak power of the outer beam. R_{hohl} is the radius where the 50° beams intersect the frustraum wall, and CCR is the minimum case-to-capsule ratio, calculated as the outer radius of the capsule, r_{cap}, divided by the closest radius of the frustraum to the capsule surface. The y value is calculated using the measured P2(μm) and then adjusting for the changes in P2. The first adjustment accounts for the peak cone fraction difference from 33%, calculated as -100*(0.33-CF)*3.5. Another adjustment accounts considers the impact of cross beam energy transfer between the inner and outer cones, calculated as -(δλ in Å)*38 μm/Å. In this empirical model, it is assumed that there is no change in P2 due to the four-color delta lambda (wavelength difference between the outer cones), but only from the two-color delta lambda (wavelength difference between the inner and average of the outer cones). The final adjustment in P2 accounts for the outer beam spot motion from the initial average outer beam spot angle, θ_{init}, to the average outer beam spot angle at peak power, that depends on pulse length, calculated here as θ_{pp}, -6.5(θ_{init}- 48.6°). For this adjustment, it is assumed that the walls are moving radially inward at ~71 μm/ns, and the parameter currently set 48.6° is used to shift all of the data points along the y axis. As this parameter is changed all of the data shifts by the same amount along the y-axis. The value of 48.6° puts the frustraum data at approximately the same y value as their cylindrical counterparts

III. EFFICIENCY IMPROVEMENTS

The efficiency improvements of the smaller wall area frustraum compared to the HyE cylindrical hohlraum are evident in several measurements. For example, Figures 3 and 6 demonstrate that the same first shock velocity can be obtained in the Frustraum 780 and 820 geometries with less picket power compared to what is required for a capsule driven in the HyE cylindrical hohlraum, 11.24 mm long by 6.4 mm in diameter, with the same 3.1 mm LEHs. This efficiency gain is further highlighted by examining the peak x-ray flux measured by the Dante diagnostic, which observes the plasma heated by the lasers hitting the hohlraum wall, and the x-ray emission from the hohlraum walls and the plasma as shown in Figure 11. The data indicates that the frustraum 780 platform exhibits a 25% higher (peak x-ray flux)$^{7/8}$ at the same equivalent gold laser energy as the HyE hohlraum, while the 820 platform shows a 14% higher (peak x-ray flux)$^{7/8}$.

A campaign denoted hohlraum scan was conducted on the NIF, in which an 1100 μm I.R. HDC capsule was placed inside the same cylindrical hohlraum as the current HyE campaign, but with varying LEH sizes. This setup allowed for a direct comparison of the efficiency by measuring the acceleration time of capsules originating from the same batch as the hohlraum scan campaign. Figure 12 displays the acceleration times from the 780 and 820 frustraum campaigns, as well as from the hohlraum scan campaign. The acceleration time, t_{acc}, represents the time from the beginning of peak power to 400 ps before bang time and signifies the acceleration time of the capsule. In simulations, the implosion time of the capsule, v_{imp}, can be expressed in terms of the peak hohlraum temperature, T_r, as

$$v_{imp} \sim T_r^{2.2} \sim R/t_{acc}, \quad (4$$

where R is the initial radius of the capsule.[12] The laser energy, E_L, can also be expressed in terms of the radiation temperature as $E_L \sim T_r^{3.5}$. Hence, the acceleration time should scale as $t_{acc} \sim E_L^{-2.2/3.5} \sim E_L^{-0.63}$. This scaling agrees very well with the data from the hohlraum scan campaign. For this plot, the effective energy of the 2D-ConA experiments was reduced by 50 kJ to account for losses in the two large uncoated windows in this platform compared with the symmetry or symcap experiments. In the hohlraum scan campaign, the effective energy was also reduced for experiments with larger LEH sizes than 3.1 mm, according to the effective loss area from Eq. 1, assuming a wall albedo of 0.85. Fig. 11 demonstrates that the same acceleration time, for capsules from the same batch, can be achieved in the 780 frustraum with ~18% less energy and in the 820 frustraum with ~14% less energy relative to the hohlraum scan experiment at 1.7 MJ and with the same 3.1 mm LEH as the frustraum campaigns.

Similarly, we can compare the ion temperature obtained using the same gas fill and pressure between the three campaigns, a mixture of 67%/33% D^3He at 2164 Torr. Figure 13 indicates that there is an ~240 eV higher ion temperature, 3.96±0.14 vs. 3.7 keV±0.14, driven in the frustraum 820 campaign compared to the hohlraum scan campaign at the same equivalent laser energy.

IV. CRYOGENIC LAYER DESIGN

The frustraum layered implosion design is discussed in greater detail in another article.[13] The design is an approximate hydroscale of the capsules used in the HyE experiment (N221204)[14] and in the Iraum experiment (N211009). In a hydroscale, the capsule dimensions are scaled with the scale factor, S, and the tungsten perentage (W %) is scaled inversely with the square of the scale factor, S^{-2}.[8] Table 1 compares the three capsule designs.

All early experiments with HDC capsules utilized microcrystalline capsules, which have larger grain boundary structures than nanocrystalline HDC capsules. However, they were easier to control in terms of capsule quality at that time. Nanocrystalline capsules offer several advantages, including smaller grain-boundary structures. Additionally, they exhibit an intriguing property wherein the density decreases with increasing W dopant at low atom percentages of W, but then begins to increase again around 0.3% W.[15] This characteristic allows for the selection of a W dopant level of ~0.51%, which matches the density of undoped HDC. For the capsule designs in the frustraum 1100 campaign, we opted for a doped layer of ~0.51% W to minimize the density difference between the doped and undoped HDC regions of the capsule. This should mitigate hydrodynamic instabilities at the interfaces between doped and undoped HDC regions of the capsule in the initial shock traversal phase of the pulse before the M-band (> 1.8 keV) fraction is large. The thickness of the layer is then chosen to achieve the desired areal density of W required to maintain a stable Atwood number between ablator and fuel during peak power when the M-band fraction reaches 20%.

Integrated and capsule-only radiation hydrodynamic codes have been used to simulate both the N221204 HyE implosion and the frustraum design featuring with the larger 1100 μm capsule. The 1-D capsule-only simulation results are presented in Table 2. The frustraum simulation utilizes 1.85 MJ of laser energy compared with 2.05 MJ for N221204. The yield increases by ~28% ($S^{4.4}$), the capsule absorbed energy by ~15% (S^3), and the hotspot pressure and energy by ~10%. The overall generalized Lawson parameter experiences an increase of ~19%.

V. SUMMARY

In this article, we present our efforts to enhance the efficiency of the frustraum in comparison to the cylindrical hohlraums currently employed at the National Ignition Facility. This was achieved by reducing the overall size of the frustraum by approximately 15% compared to our previous experiments.[3] Additionally, we decreased the capsule size to an inner radius of 1.1 mm and employed a lower adiabat pulse shape, in contrast with our prior work in a larger scale frustraum.

The 8.2 mm diameter frustraum with a 25° wall angle demonstrated a roughly 14% improvement in efficiency relative to cylindrical hohlraum experiments conducted in a 6.4 mm diameter by 11.24 mm long cylinders, both with 3.1 mm LEHs. During these experiments, the backscatter from these frustraums remained low, with over 99% laser coupling, at the power level of 430 TW and energy levels of 1.6 MJ. We observed an ~240 eV increase in the ion energy for a given laser energy compared with the cylindrical experiments. By transitioning from a 23° to a 25° wall angle and utilizing 1.25 Å of delta lambda, we successfully demonstrated a prolate implosion at 1.6 MJ.

Future experiments will focus on improving inflight P4 measurements and refining the 2D-ConA platform in preparation for layered implosions. Efforts will also be directed towards understanding and mitigating P2 swings, inflight P4, and the formation of polar ice caps/jets observed in integrated radiation hydrodynamics simulations.

Current one-dimensional capsule-only simulations predict a $(1.1/1.05)^{4.4}$ ~ 25% increase in maximum yield over the current 1.05 mm capsules used in cylindrical layered implosions.This is approximately the no-alpha increase in yield expected from hydroscaling.[16] Higher yield gains are expected when include yield amplification by alpha heating. Additionally, these simulations suggest improved robustness to mix and low mode perturbations, attributed to the higher generalized Lawson parameter.

ACKNOWLEDGMENTS

We wish to thank the NIF operations team. This work was performed under the auspices of the U.S. Department of Energy by Lawrence Livermore National Laboratory under Contract DE-AC52-07NA27344 and by General Atomics under contract DE-NA0001808. The data that support the findings of this study are available from the corresponding author upon reasonable request.

Appendix A   Mode 1 correction for the down-scattered ratio, DSR

In our previous article, we utilized a simplified expression for the mode 1 reduction in the DSR, given by DSR = DSR_0/(1-(P1/P0)^2). Figure A1 illustrates the simulated values of DSR (black circles) as a function of P1/P0 with increasing mode 1. The simplified expression DSR_0/(1-(P1/P0)^2) is represented by the dashed red line. A more accurate fit for the degradation caused by mode 1 is achieved using the expression DSR = DSR_0/(1-1.5*(P1/P0)$^{2.7}$). This improved expression is depicted as the dashed blue line in Appendix Figure A1.

REFERENCES

[1] J. Lindl, Development of the indirect-drive approach to inertial confinement fusion and the target physics basis for ignition and gain, Phys. Plasmas, 2 (1995) 3933-4024.
[2] S. Atzeni, J. Meyer-ter-Vehn, The Physics of Inertial Fusion, Oxford University Press2008.
[3] K.L. Baker, P.A. Amendt, J.S. Ross, V.A. Smalyuk, O.L. Landen, D.D. Ho, S. Khan, S.W. Haan, J.D. Lindl, D. Mariscal, J.L. Milovich, S. MacLaren, Y. Ping, D.J. Strozzi, R. Bionta, D. Casey, P.M. Celliers, D. Fittinghoff, H. Geppert-Kleinrath, V. Geppert-Kleinrath, K.D. Hahn, M. Gatu Johnson, Y. Kim, K. Meaney, M. Millot, R. Nora, P. Volegov, C. Wilde, First Large Capsule Implosions in a Frustum-shaped Hohlraum Phys. Plasmas, 30 (2023) 092708.
[4] P. Amendt, D. Ho, Y. Ping, V. Smalyuk, S. Khan, J. Lindl, D. Strozzi, R. Tommasini, M. Belyaev, C. Cerjan, O. Jones, W. Kruer, N. Meezan, H. Robey, F. Tsung, C. Weber, C. Young, Ultra-high (>30%) coupling efficiency designs for demonstrating central hot-spot ignition on the National Ignition Facility using a Frustraum, Physics of Plasmas, 26 (2019) 082707.
[5] J.D. Moody, O.L. Landen, L. Divol, S. LePape, P. Michel, R.P.J. Town, G. Hall, K. Widmann, A. Moore, Semi-empirical “leaky-bucket” model of laser-driven x-ray cavities, Physics of Plasmas, 24 (2017).

[6] R. Tommasini , D.T. Casey, D. Clark, A. Do , K.L. Baker, O.L. Landen , V.A. Smalyuk, C. Weber, B. Bachmann, E. Hartouni, S. Kerr, C. Krauland, E.V. Marley, M. Millot , J. Milovich, R.C. Nora , A.E. Pak, D. Schlossberg, B. Woodworth, T.M. Briggs, D.M. Holunga , A. Nikroo, M. Stadermann, Increased compression in HDC-based ablator implosions using modified drive profile, PHYSICAL REVIEW RESEARCH, 5 (2023) L042034.
[7] A. Do, D.T. Casey, D.S. Clark, B. Bachmann, K.L. Baker, T. Braun, T.M. Briggs, T.D. Chapman, M. Celliers, H. Chen, C. Choate, E.L. Dewald, L. Divol, G. Fathi, D.N. Fittinghoff, G.N. Hall, E. Hartouni, D.M. Holunga, S.F. Khan, A.L. Kritcher, O.L. Landen, A.G. MacPhee, M. Millot, E.V. Marley, J.L. Milovich, A. Nikroo, A.E. Pak, D.J. Schlossberg, V.A. Smalyuk, M. Stadermann, D.J. Strozzi, R. Tommasini, C.R. Weber, B.N. Woodworth, D.K. Yanagisawa, N.W. Birge, C.R. Danly, M. Durocher, M.S. Freeman, H. Geppert-Kleinrath, V. Geppert-Kleinrath, Y. Kim, K.D. Meaney, C.H. Wilde, M.G. Johnson, A. Allen, M. Ratledge, C. Kong, T. Fehrenbach, C. Wild, Measurements of improved stability to achieve higher fuel compression in ICF, Phys. Plasmas, 30 (2023) 112703.
[8] K.L. Baker, O. Jones, C. Weber, D. Clark, P.K. Patel, C.A. Thomas, O.L. Landen, R. Nora, G.J. Anderson, J. Gaffney, S. MacLaren, D.T. Casey, T. Döppner, E.L. Dewald, R. Tommasini, B.K. Spears, J. Salmonson, M. Hohenberger, S. Khan, A. Zylstra, A. Kritcher, P. Amendt, V. Smalyuk, J. Lindl, C. Young, J.S. Ross, D. Ho, O.A. Hurricane, D.A. Callahan, T. Woods, J.L. Milovich, D.J. Strozzi, B. Bachmann, R. Bionta, P.M. Celliers, D. Fittinghoff, R. Hatarik, M. Gatu Johnson, K. Meaney, M. Millot, P.L. Volegov, C. Wilde, Hydroscaling indirect-drive implosions on the National Ignition Facility, Physics of Plasmas, 29 (2022) 062705.
[9] J.D. Lindl, P. Amendt, R.L. Berger, S.G. Glendinning, S.H. Glenzer, S.W. Haan, R.L. Kauffman, O.L. Landen, L.J. Suter, The physics basis for ignition using indirect-drive targets on the National Ignition Facility, Physics of Plasmas, 11 (2004) 339-491.
[10] H. Abu-Shawareb, R. Acree, P. Adams, J. Adams, B. Addis, R. Aden, P. Adrian, B.B. Afeyan, M. Aggleton, L. Aghaian, A. Aguirre, D. Aikens, J. Akre, F. Albert, M. Albrecht, B.J. Albright, J. Albritton, J. Alcala, C. Alday, D.A. Alessi, N. Alexander, J. Alfonso, N. Alfonso, E. Alger, S.J. Ali, Z.A. Ali, W.E. Alley, P. Amala, P.A. Amendt, P. Amick, S. Ammula, C. Amorin, D.J. Ampleford, R.W. Anderson, T. Anklam, N. Antipa, B. Appelbe, C. Aracne-Ruddle, E. Araya, M. Arend, P. Arnold, T. Arnold, J. Asay, L.J. Atherton, D. Atkinson, R. Atkinson, J.M. Auerbach, B. Austin, L. Auyang, A.S. Awwal, J. Ayers, S. Ayers, T. Ayers, S. Azevedo, B. Bachmann, C.A. Back, J. Bae, D.S. Bailey, J. Bailey, T. Baisden, K.L. Baker, H. Baldis, D. Barber, M. Barberis, D. Barker, A. Barnes, C.W. Barnes, M.A. Barrios, C. Barty, I. Bass, S.H. Batha, S.H. Baxamusa, G. Bazan, J.K. Beagle, R. Beale, B.R. Beck, J.B. Beck, M. Bedzyk, R.G. Beeler, R.G. Beeler, W. Behrendt, L. Belk, P. Bell, M. Belyaev, J.F. Benage, G. Bennett, L.R. Benedetti, L.X. Benedict, R. Berger, T. Bernat, L.A. Bernstein, B. Berry, L. Bertolini, G. Besenbruch, J. Betcher, R. Bettenhausen, R. Betti, B. Bezzerides, S.D. Bhandarkar, R. Bickel, J. Biener, T. Biesiada, K. Bigelow, J. Bigelow-Granillo, V. Bigman, R.M. Bionta, N.W. Birge, M. Bitter, A.C. Black, R. Bleile, D.L. Bleuel, E. Bliss, E. Bliss, B. Blue, T. Boehly, K. Boehm, C.D. Boley, R. Bonanno, E.J. Bond, T. Bond, M.J. Bonino, M. Borden, J.L. Bourgade, J. Bousquet, J. Bowers, M. Bowers, R. Boyd, A. Bozek, D.K. Bradley, K.S. Bradley, P.A. Bradley, L. Bradley, L. Brannon, P.S. Brantley, D. Braun, T. Braun, K. Brienza-Larsen, T.M. Briggs, J. Britten, E.D. Brooks, D. Browning, M.W. Bruhn, T.A. Brunner, H. Bruns, G. Brunton, B. Bryant, T. Buczek, J. Bude, L. Buitano, S. Burkhart, J. Burmark, A. Burnham, R. Burr, L.E. Busby, B. Butlin, R. Cabeltis, M. Cable, W.H. Cabot, B. Cagadas, J. Caggiano, R. Cahayag, S.E. Caldwell, S. Calkins, D.A. Callahan, J. Calleja-Aguirre, L. Camara, D. Camp, E.M. Campbell, J.H. Campbell,

B. Carey, R. Carey, K. Carlisle, L. Carlson, L. Carman, J. Carmichael, A. Carpenter, C. Carr, J.A. Carrera, D. Casavant, A. Casey, D.T. Casey, A. Castillo, E. Castillo, J.I. Castor, C. Castro, W. Caughey, R. Cavitt, J. Celeste, P.M. Celliers, C. Cerjan, G. Chandler, B. Chang, C. Chang, J. Chang, L. Chang, R. Chapman, T. Chapman, L. Chase, H. Chen, H. Chen, K. Chen, L.Y. Chen, B. Cheng, J. Chittenden, C. Choate, J. Chou, R.E. Chrien, M. Chrisp, K. Christensen, M. Christensen, A.R. Christopherson, M. Chung, J.A. Church, A. Clark, D.S. Clark, K. Clark, R. Clark, L. Claus, B. Cline, J.A. Cline, J.A. Cobble, K. Cochrane, B. Cohen, S. Cohen, M.R. Collette, G. Collins, L.A. Collins, T.J.B. Collins, A. Conder, B. Conrad, M. Conyers, A.W. Cook, D. Cook, R. Cook, J.C. Cooley, G. Cooper, T. Cope, S.R. Copeland, F. Coppari, J. Cortez, J. Cox, D.H. Crandall, J. Crane, R.S. Craxton, M. Cray, A. Crilly, J.W. Crippen, D. Cross, M. Cuneo, G. Cuotts, C.E. Czajka, D. Czechowicz, T. Daly, P. Danforth, R. Darbee, B. Darlington, P. Datte, L. Dauffy, G. Davalos, S. Davidovits, P. Davis, J. Davis, S. Dawson, R.D. Day, T.H. Day, M. Dayton, C. Deck, C. Decker, C. Deeney, K.A. DeFriend, G. Deis, N.D. Delamater, J.A. Delettrez, R. Demaret, S. Demos, S.M. Dempsey, R. Desjardin, T. Desjardins, M.P. Desjarlais, E.L. Dewald, J. DeYoreo, S. Diaz, G. Dimonte, T.R. Dittrich, L. Divol, S.N. Dixit, J. Dixon, E.S. Dodd, D. Dolan, A. Donovan, M. Donovan, T. Doppner, C. Dorrer, N. Dorsano, M.R. Douglas, D. Dow, J. Downie, E. Downing, M. Dozieres, V. Draggoo, D. Drake, R.P. Drake, T. Drake, G. Dreifuerst, D.F. DuBois, P.F. DuBois, G. Dunham, R. Dylla-Spears, A.K.L. Dymoke-Bradshaw, B. Dzenitis, C. Ebbers, M. Eckart, S. Eddinger, D. Eder, D. Edgell, M.J. Edwards, P. Efthimion, J.H. Eggert, B. Ehrlich, P. Ehrmann, S. Elhadj, C. Ellerbee, N.S. Elliott, C.L. Ellison, F. Elsner, M. Emerich, K. Engelhorn, T. England, E. English, P. Epperson, R. Epstein, G. Erbert, M.A. Erickson, D.J. Erskine, A. Erlandson, R.J. Espinosa, C. Estes, K.G. Estabrook, S. Evans, A. Fabyan, J. Fair, R. Fallejo, N. Farmer, W.A. Farmer, M. Farrell, V.E. Fatherley, M. Fedorov, E. Feigenbaum, M. Feit, W. Ferguson, J.C. Fernandez, A. Fernandez-Panella, S. Fess, J.E. Field, C.V. Filip, J.R. Fincke, T. Finn, S.M. Finnegan, R.G. Finucane, M. Fischer, A. Fisher, J. Fisher, B. Fishler, D. Fittinghoff, P. Fitzsimmons, M. Flegel, K.A. Flippo, J. Florio, J. Folta, P. Folta, L.R. Foreman, C. Forrest, A. Forsman, J. Fooks, M. Foord, R. Fortner, K. Fournier, D.E. Fratanduono, N. Frazier, T. Frazier, C. Frederick, M.S. Freeman, J. Frenje, D. Frey, G. Frieders, S. Friedrich, D.H. Froula, J. Fry, T. Fuller, J. Gaffney, S. Gales, B. Le Galloudec, K.K. Le Galloudec, A. Gambhir, L. Gao, W.J. Garbett, A. Garcia, C. Gates, E. Gaut, P. Gauthier, Z. Gavin, J. Gaylord, M. Geissel, F. Genin, J. Georgeson, H. Geppert-Kleinrath, V. Geppert-Kleinrath, N. Gharibyan, J. Gibson, C. Gibson, E. Giraldez, V. Glebov, S.G. Glendinning, S. Glenn, S.H. Glenzer, S. Goade, P.L. Gobby, S.R. Goldman, B. Golick, M. Gomez, V. Goncharov, D. Goodin, P. Grabowski, E. Grafil, P. Graham, J. Grandy, E. Grasz, F. Graziani, G. Greenman, J.A. Greenough, A. Greenwood, G. Gregori, T. Green, J.R. Griego, G.P. Grim, J. Grondalski, S. Gross, J. Guckian, N. Guler, B. Gunney, G. Guss, S. Haan, J. Hackbarth, L. Hackel, R. Hackel, C. Haefner, C. Hagmann, K.D. Hahn, S. Hahn, B.J. Haid, B.M. Haines, B.M. Hall, C. Hall, G.N. Hall, M. Hamamoto, S. Hamel, C.E. Hamilton, B.A. Hammel, J.H. Hammer, G. Hampton, A. Hamza, A. Handler, S. Hansen, D. Hanson, R. Haque, D. Harding, E. Harding, J.D. Hares, D.B. Harris, J.A. Harte, E.P. Hartouni, R. Hatarik, S. Hatchett, A.A. Hauer, M. Havre, R. Hawley, J. Hayes, J. Hayes, S. Hayes, A. Hayes-Sterbenz, C.A. Haynam, D.A. Haynes, D. Headley, A. Heal, J.E. Heebner, S. Heerey, G.M. Heestand, R. Heeter, N. Hein, C. Heinbockel, C. Hendricks, M. Henesian, J. Heninger, J. Henrikson, E.A. Henry, E.B. Herbold, M.R. Hermann, G. Hermes, J.E. Hernandez, V.J. Hernandez, M.C. Herrmann, H.W. Herrmann, O.D. Herrera, D. Hewett, R. Hibbard, D.G. Hicks, D. Hill, K. Hill, T. Hilsabeck, D.E. Hinkel, D.D. Ho, V.K. Ho, J.K. Hoffer, N.M. Hoffman, M. Hohenberger, M. Hohensee, W. Hoke, D.

Holdener, F. Holdener, J.P. Holder, B. Holko, D. Holunga, J.F. Holzrichter, J. Honig, D. Hoover, D. Hopkins, L. Berzak Hopkins, M. Hoppe, M.L. Hoppe, J. Horner, R. Hornung, C.J. Horsfield, J. Horvath, D. Hotaling, R. House, L. Howell, W.W. Hsing, S.X. Hu, H. Huang, J. Huckins, H. Hui, K.D. Humbird, J. Hund, J. Hunt, O.A. Hurricane, M. Hutton, K.H. Huynh, L. Inandan, C. Iglesias, I.V. Igumenshchev, N. Izumi, M. Jackson, J. Jackson, S.D. Jacobs, G. James, K. Jancaitis, J. Jarboe, L.C. Jarrott, D. Jasion, J. Jaquez, J. Jeet, A.E. Jenei, J. Jensen, J. Jimenez, R. Jimenez, D. Jobe, Z. Johal, H.M. Johns, D. Johnson, M.A. Johnson, M. Gatu Johnson, R.J. Johnson, S. Johnson, S.A. Johnson, T. Johnson, K. Jones, O. Jones, M. Jones, R. Jorge, H.J. Jorgenson, M. Julian, B.I. Jun, R. Jungquist, J. Kaae, N. Kabadi, D. Kaczala, D. Kalantar, K. Kangas, V.V. Karasiev, M. Karasik, V. Karpenko, A. Kasarky, K. Kasper, R. Kauffman, M.I. Kaufman, C. Keane, L. Keaty, L. Kegelmeyer, P.A. Keiter, P.A. Kellett, J. Kellogg, J.H. Kelly, S. Kemic, A.J. Kemp, G.E. Kemp, G.D. Kerbel, D. Kershaw, S.M. Kerr, T.J. Kessler, M.H. Key, S.F. Khan, H. Khater, C. Kiikka, J. Kilkenny, Y. Kim, Y.J. Kim, J. Kimko, M. Kimmel, J.M. Kindel, J. King, R.K. Kirkwood, L. Klaus, D. Klem, J.L. Kline, J. Klingmann, G. Kluth, P. Knapp, J. Knauer, J. Knipping, M. Knudson, D. Kobs, J. Koch, T. Kohut, C. Kong, J.M. Koning, P. Koning, S. Konior, H. Kornblum, L.B. Kot, B. Kozioziemski, M. Kozlowski, P.M. Kozlowski, J. Krammen, N.S. Krasheninnikova, B. Kraus, W. Krauser, J.D. Kress, A.L. Kritcher, E. Krieger, J.J. Kroll, W.L. Kruer, M.K.G. Kruse, S. Kucheyev, M. Kumbera, S. Kumpan, J. Kunimune, B. Kustowski, T.J.T. Kwan, G.A. Kyrala, S. Laffite, M. Lafon, K. LaFortune, B. Lahmann, B. Lairson, O.L. Landen, J. Langenbrunner, L. Lagin, T. Land, M. Lane, D. Laney, A.B. Langdon, S.H. Langer, A. Langro, N.E. Lanier, T.E. Lanier, D. Larson, B.F. Lasinski, D. Lassle, D. LaTray, G. Lau, N. Lau, C. Laumann, A. Laurence, T.A. Laurence, J. Lawson, H.P. Le, R.R. Leach, L. Leal, A. Leatherland, K. LeChien, B. Lechleiter, A. Lee, M. Lee, T. Lee, R.J. Leeper, E. Lefebvre, J.P. Leidinger, B. LeMire, R.W. Lemke, N.C. Lemos, S. Le Pape, R. Lerche, S. Lerner, S. Letts, K. Levedahl, T. Lewis, C.K. Li, H. Li, J. Li, W. Liao, Z.M. Liao, D. Liedahl, J. Liebman, G. Lindford, E.L. Lindman, J.D. Lindl, H. Loey, R.A. London, F. Long, E.N. Loomis, F.E. Lopez, H. Lopez, E. Losbanos, S. Loucks, R. Lowe-Webb, E. Lundgren, A.P. Ludwigsen, R. Luo, J. Lusk, R. Lyons, T. Ma, Y. Macallop, M.J. MacDonald, B.J. MacGowan, J.M. Mack, A.J. Mackinnon, S.A. MacLaren, A.G. MacPhee, G.R. Magelssen, J. Magoon, R.M. Malone, T. Malsbury, R. Managan, R. Mancini, K. Manes, D. Maney, D. Manha, O.M. Mannion, A.M. Manuel, E. Mapoles, G. Mara, T. Marcotte, E. Marin, M.M. Marinak, C. Mariscal, D.A. Mariscal, E.F. Mariscal, E.V. Marley, J.A. Marozas, R. Marquez, C.D. Marshall, F.J. Marshall, M. Marshall, S. Marshall, J. Marticorena, D. Martinez, I. Maslennikov, D. Mason, R.J. Mason, L. Masse, W. Massey, P.E. Masson-Laborde, N.D. Masters, D. Mathisen, E. Mathison, J. Matone, M.J. Matthews, C. Mattoon, T.R. Mattsson, K. Matzen, C.W. Mauche, M. Mauldin, T. McAbee, M. McBurney, T. McCarville, R.L. McCrory, A.M. McEvoy, C. McGuffey, M. McInnis, P. McKenty, M.S. McKinley, J.B. McLeod, A. McPherson, B. McQuillan, M. Meamber, K.D. Meaney, N.B. Meezan, R. Meissner, T.A. Mehlhorn, N.C. Mehta, J. Menapace, F.E. Merrill, B.T. Merritt, E.C. Merritt, D.D. Meyerhofer, S. Mezyk, R.J. Mich, P.A. Michel, D. Milam, C. Miller, D. Miller, D.S. Miller, E. Miller, E.K. Miller, J. Miller, M. Miller, P.E. Miller, T. Miller, W. Miller, V. Miller-Kamm, M. Millot, J.L. Milovich, P. Minner, J.L. Miquel, S. Mitchell, K. Molvig, R.C. Montesanti, D.S. Montgomery, M. Monticelli, A. Montoya, J.D. Moody, A.S. Moore, E. Moore, M. Moran, J.C. Moreno, K. Moreno, B.E. Morgan, T. Morrow, J.W. Morton, E. Moses, K. Moy, R. Muir, M.S. Murillo, J.E. Murray, J.R. Murray, D.H. Munro, T.J. Murphy, F.M. Munteanu, J. Nafziger, T. Nagayama, S.R. Nagel, R. Nast, R.A. Negres, A. Nelson, D. Nelson, J. Nelson, S. Nelson, S. Nemethy, P.

Neumayer, K. Newman, M. Newton, H. Nguyen, J.G. Di Nicola, P. Di Nicola, C. Niemann, A. Nikroo, P.M. Nilson, A. Nobile, V. Noorai, R. Nora, M. Norton, M. Nostrand, V. Note, S. Novell, P.F. Nowak, A. Nunez, R.A. Nyholm, M. O'Brien, A. Oceguera, J.A. Oertel, J. Okui, B. Olejniczak, J. Oliveira, P. Olsen, B. Olson, K. Olson, R.E. Olson, Y.P. Opachich, N. Orsi, C.D. Orth, M. Owen, S. Padalino, E. Padilla, R. Paguio, S. Paguio, J. Paisner, S. Pajoom, A. Pak, S. Palaniyappan, K. Palma, T. Pannell, F. Papp, D. Paras, T. Parham, H.S. Park, A. Pasternak, S. Patankar, M.V. Patel, P.K. Patel, R. Patterson, S. Patterson, B. Paul, M. Paul, E. Pauli, O.T. Pearce, J. Pearcy, B. Pedrotti, A. Peer, L.J. Pelz, B. Penetrante, J. Penner, A. Perez, L.J. Perkins, E. Pernice, T.S. Perry, S. Person, D. Petersen, T. Petersen, D.L. Peterson, E.B. Peterson, J.E. Peterson, J.L. Peterson, K. Peterson, R.R. Peterson, R.D. Petrasso, F. Philippe, T.J. Phipps, E. Piceno, Y. Ping, L. Pickworth, J. Pino, R. Plummer, G.D. Pollack, S.M. Pollaine, B.B. Pollock, D. Ponce, J. Ponce, J. Pontelandolfo, J.L. Porter, J. Post, O. Poujade, C. Powell, H. Powell, G. Power, M. Pozulp, M. Prantil, M. Prasad, S. Pratuch, S. Price, K. Primdahl, S. Prisbrey, R. Procassini, A. Pruyne, B. Pudliner, S.R. Qiu, K. Quan, M. Quinn, J. Quintenz, P.B. Radha, F. Rainer, J.E. Ralph, K.S. Raman, R. Raman, P. Rambo, S. Rana, A. Randewich, D. Rardin, M. Ratledge, N. Ravelo, F. Ravizza, M. Rayce, A. Raymond, B. Raymond, B. Reed, C. Reed, S. Regan, B. Reichelt, V. Reis, S. Reisdorf, V. Rekow, B.A. Remington, A. Rendon, W. Requieron, M. Rever, H. Reynolds, J. Reynolds, J. Rhodes, M. Rhodes, M.C. Richardson, B. Rice, N.G. Rice, R. Rieben, A. Rigatti, S. Riggs, H.G. Rinderknecht, K. Ring, B. Riordan, R. Riquier, C. Rivers, D. Roberts, V. Roberts, G. Robertson, H.F. Robey, J. Robles, P. Rocha, G. Rochau, J. Rodriguez, S. Rodriguez, M. Rosen, M. Rosenberg, G. Ross, J.S. Ross, P. Ross, J. Rouse, D. Rovang, A.M. Rubenchik, M.S. Rubery, C.L. Ruiz, M. Rushford, B. Russ, J.R. Rygg, B.S. Ryujin, R.A. Sacks, R.F. Sacks, K. Saito, T. Salmon, J.D. Salmonson, J. Sanchez, S. Samuelson, M. Sanchez, C. Sangster, A. Saroyan, J. Sater, A. Satsangi, S. Sauers, R. Saunders, J.P. Sauppe, R. Sawicki, D. Sayre, M. Scanlan, K. Schaffers, G.T. Schappert, S. Schiaffino, D.J. Schlossberg, D.W. Schmidt, M.J. Schmitt, D.H.G. Schneider, M.B. Schneider, R. Schneider, M. Schoff, M. Schollmeier, M. Scholmerich, C.R. Schroeder, S.E. Schrauth, H.A. Scott, I. Scott, J.M. Scott, R.H.H. Scott, C.R. Scullard, T. Sedillo, F.H. Seguin, W. Seka, J. Senecal, S.M. Sepke, L. Seppala, K. Sequoia, J. Severyn, J.M. Sevier, N. Sewell, S. Seznec, R.C. Shah, J. Shamlian, D. Shaughnessy, M. Shaw, R. Shaw, C. Shearer, R. Shelton, N. Shen, M.W. Sherlock, A.I. Shestakov, E.L. Shi, S.J. Shin, N. Shingleton, W. Shmayda, M. Shor, M. Shoup, C. Shuldberg, L. Siegel, F.J. Silva, A.N. Simakov, B.T. Sims, D. Sinars, P. Singh, H. Sio, K. Skulina, S. Skupsky, S. Slutz, M. Sluyter, V.A. Smalyuk, D. Smauley, R.M. Smeltser, C. Smith, I. Smith, J. Smith, L. Smith, R. Smith, R. Sohn, S. Sommer, C. Sorce, M. Sorem, J.M. Soures, M.L. Spaeth, B.K. Spears, S. Speas, D. Speck, R. Speck, J. Spears, T. Spinka, P.T. Springer, M. Stadermann, B. Stahl, J. Stahoviak, L.G. Stanton, R. Steele, W. Steele, D. Steinman, R. Stemke, R. Stephens, S. Sterbenz, P. Sterne, D. Stevens, J. Stevers, C.B. Still, C. Stoeckl, W. Stoeffl, J.S. Stolken, C. Stolz, E. Storm, G. Stone, S. Stoupin, E. Stout, I. Stowers, R. Strauser, H. Streckart, J. Streit, D.J. Strozzi, T. Suratwala, G. Sutcliffe, L.J. Suter, S.B. Sutton, V. Svidzinski, G. Swadling, W. Sweet, A. Szoke, M. Tabak, M. Takagi, A. Tambazidis, V. Tang, M. Taranowski, L.A. Taylor, S. Telford, W. Theobald, M. Thi, A. Thomas, C.A. Thomas, I. Thomas, R. Thomas, I.J. Thompson, A. Thongstisubskul, C.B. Thorsness, G. Tietbohl, R.E. Tipton, M. Tobin, N. Tomlin, R. Tommasini, A.J. Toreja, J. Torres, R.P.J. Town, S. Townsend, J. Trenholme, A. Trivelpiece, C. Trosseille, H. Truax, D. Trummer, S. Trummer, T. Truong, D. Tubbs, E.R. Tubman, T. Tunnell, D. Turnbull, R.E. Turner, M. Ulitsky, R. Upadhye, J.L. Vaher, P. VanArsdall, D. VanBlarcom, M. Vandenboomgaerde, R. VanQuinlan, B.M. Van Wonterghem, W.S. Varnum, A.L.

Velikovich, A. Vella, C.P. Verdon, B. Vermillion, S. Vernon, R. Vesey, J. Vickers, R.M. Vignes, M. Visosky, J. Vocke, P.L. Volegov, S. Vonhof, R. Von Rotz, H.X. Vu, M. Vu, D. Wall, J. Wall, R. Wallace, B. Wallin, D. Walmer, C.A. Walsh, C.F. Walters, C. Waltz, A. Wan, A. Wang, Y. Wang, J.S. Wark, B.E. Warner, J. Watson, R.G. Watt, P. Watts, J. Weaver, R.P. Weaver, S. Weaver, C.R. Weber, P. Weber, S.V. Weber, P. Wegner, B. Welday, L. Welser-Sherrill, K. Weiss, K. Widmann, G.F. Wheeler, W. Whistler, R.K. White, H.D. Whitley, P. Whitman, M.E. Wickett, C. Widmayer, J. Wiedwald, R. Wilcox, S. Wilcox, C. Wild, B.H. Wilde, C.H. Wilde, K. Wilhelmsen, M.D. Wilke, H. Wilkens, P. Wilkins, S.C. Wilks, E.A. Williams, G.J. Williams, W. Williams, W.H. Williams, D.C. Wilson, B. Wilson, E. Wilson, R. Wilson, S. Winters, J. Wisoff, M. Wittman, J. Wolfe, A. Wong, K.W. Wong, L. Wong, N. Wong, R. Wood, D. Woodhouse, J. Woodruff, D.T. Woods, S. Woods, B.N. Woodworth, E. Wooten, A. Wootton, K. Work, J.B. Workman, J. Wright, M. Wu, C. Wuest, F.J. Wysocki, H. Xu, M. Yamaguchi, B. Yang, S.T. Yang, J. Yatabe, C.B. Yeamans, B.C. Yee, S.A. Yi, L. Yin, B. Young, C.S. Young, C.V. Young, P. Young, K. Youngblood, R. Zacharias, G. Zagaris, N. Zaitseva, F. Zaka, F. Ze, B. Zeiger, M. Zika, G.B. Zimmerman, T. Zobrist, J.D. Zuegel, A.B. Zylstra, I.C.F.C. Indirect Drive, Lawson Criterion for Ignition Exceeded in an Inertial Fusion Experiment, Phys Rev Lett, 129 (2022) 075001.

[11] A.L. Kritcher, A.B. Zylstra, D.A. Callahan, O.A. Hurricane, C.R. Weber, D.S. Clark, C.V. Young, J.E. Ralph, D.T. Casey, A. Pak, O.L. Landen, B. Bachmann, K.L. Baker, L. Berzak Hopkins, S.D. Bhandarkar, J. Biener, R.M. Bionta, N.W. Birge, T. Braun, T.M. Briggs, P.M. Celliers, H. Chen, C. Choate, L. Divol, T. Döppner, D. Fittinghoff, M.J. Edwards, M. Gatu Johnson, N. Gharibyan, S. Haan, K.D. Hahn, E. Hartouni, D.E. Hinkel, D.D. Ho, M. Hohenberger, J.P. Holder, H. Huang, N. Izumi, J. Jeet, O. Jones, S.M. Kerr, S.F. Khan, H. Geppert Kleinrath, V. Geppert Kleinrath, C. Kong, K.M. Lamb, S. Le Pape, N.C. Lemos, J.D. Lindl, B.J. MacGowan, A.J. Mackinnon, A.G. MacPhee, E.V. Marley, K. Meaney, M. Millot, A.S. Moore, K. Newman, J.M.G. Di Nicola, A. Nikroo, R. Nora, P.K. Patel, N.G. Rice, M.S. Rubery, J. Sater, D.J. Schlossberg, S.M. Sepke, K. Sequoia, S.J. Shin, M. Stadermann, S. Stoupin, D.J. Strozzi, C.A. Thomas, R. Tommasini, C. Trosseille, E.R. Tubman, P.L. Volegov, C. Wild, D.T. Woods, S.T. Yang, Design of an inertial fusion experiment exceeding the Lawson criterion for ignition, Physical Review E, 106 (2022) 025201.

[12] K. Baker, C. Thomas, O. Landen, S. Haan, J. Lindl, D. Casey, C. Young, R. Nora, O. Hurricane, D. Callahan, O. Jones, L. Berzak Hopkins, S. Khan, B. Spears, S. Le Pape, N. Meezan, D. Ho, T. Döppner, D. Hinkel, E. Dewald, R. Tommasini, M. Hohenberger, C. Weber, D. Clark, D. Woods, J. Milovich, D. Strozzi, A. Kritcher, H. Robey, J. Ross, V. Smalyuk, P. Amendt, B. Bachmann, L. Benedetti, R. Bionta, P. Celliers, D. Fittinghoff, C. Goyon, R. Hatarik, N. Izumi, M. Gatu Johnson, G. Kyrala, T. Ma, K. Meaney, M. Millot, S. Nagel, P. Patel, D. Turnbull, P. Volegov, C. Yeamans, B.H. Wilde, Reaching a burning plasma and ignition using smaller capsules/Hohlraums, higher radiation temperatures, and thicker ablator/ice on the national ignition facility, Physics of Plasmas, 30 (2023) 032702.

[13] D. Ho, P. Amendt, K.L. Baker, O.L. Landen, J. Lindl, M. Marinak, D. Mariscal, H. Sio, A.L. Velikovich, G. Zimmerman, Implosions for high yield with reduced laser energy using high-efficiency Frustraums and enhanced Frustraum performance by magnetization, to be submitted to High Energy Density Physics, DOI (2024).

[14] H. Abu-Shawareb, R. Acree, P. Adams, J. Adams, B. Addis, R. Aden, P. Adrian, B.B. Afeyan, M. Aggleton, L. Aghaian, A. Aguirre, D. Aikens, J. Akre, F. Albert, M. Albrecht, B.J. Albright, J. Albritton, J. Alcala, J. C. Alday, D.A. Alessi, N. Alexander, J. Alfonso, N. Alfonso,

E. Alger, S.J. Ali, Z.A. Ali, A. Allen1, W.E. Alley, P. Amala, P.A. Amendt, P. Amick, S. Ammula, C. Amorin, D.J. Ampleford, R.W. Anderson, T. Anklam, N. Antipa, B. Appelbe, C. Aracne-Ruddle, E. Araya, T.N. Archuleta, M. Arend, P. Arnold, T. Arnold, A. Arsenlis, J. Asay, L.J. Atherton, D. Atkinson, R. Atkinson, J.M. Auerbach, B. Austin, L. Auyang, A.A.S. Awwal, N. Aybar, J. Ayers, S. Ayers, T. Ayers, S. Azevedo, B. Bachmann, C.A. Back, J. Bae, D.S. Bailey, J. Bailey, T. Baisden, K.L. Baker, H. Baldis, D. Barber, M. Barberis, D. Barker, A. Barnes, C.W. Barnes, M.A. Barrios, C. Barty, I. Bass, S.H. Batha, S.H. Baxamusa, G. Bazan, J.K. Beagle, R. Beale, B.R. Beck, J.B. Beck, M. Bedzyk, R.G. Beeler, R.G. Beeler, W. Behrendt, L. Belk, P. Bell, M. Belyaev, J.F. Benage, G. Bennett, L.R. Benedetti, L.X. Benedict, R.L. Berger, T. Bernat, L.A. Bernstein, B. Berry, L. Bertolini, G. Besenbruch, J. Betcher, R. Bettenhausen, R. Betti, B. Bezzerides, S.D. Bhandarkar, R. Bickel, J. Biener, T. Biesiada, K. Bigelow, J. Bigelow-Granillo, V. Bigman, R.M. Bionta, N.W. Birge, M. Bitter, A.C. Black, R. Bleile, D.L. Bleuel, E. Bliss, B. Blue, T. Boehly, K. Boehm, C.D. Boley, R. Bonanno, E.J. Bond, T. Bond, M.J. Bonino, M. Borden, J.-L. Bourgade, J. Bousquet, J. Bowers, M. Bowers, R. Boyd, D. Boyle, A. Bozek, D.K. Bradley, K.S. Bradley, P.A. Bradley, L. Bradley, L. Brannon, P.S. Brantley, D. Braun, T. Braun, K. Brienza-Larsen, R. Briggs, T.M. Briggs, J. Britten, E.D. Brooks, D. Browning, M.W. Bruhn, T.A. Brunner, H. Bruns, G. Brunton, B. Bryant, T. Buczek, J. Bude, L. Buitano, S. Burkhart, J. Burmark, A. Burnham, R. Burr, L.E. Busby, B. Butlin, R. Cabeltis, M. Cable, W.H. Cabot, B. Cagadas, J. Caggiano, R. Cahayag, S.E. Caldwell, S. Calkins, D.A. Callahan, J. Calleja-Aguirre, L. Camara, D. Camp, E.M. Campbell, J.H. Campbell, B. Carey, R. Carey, K. Carlisle, L. Carlson, L. Carman, J. Carmichael, A. Carpenter, C. Carr, J.A. Carrera, D. Casavant, A. Casey, D.T. Casey, A. Castillo, E. Castillo, J.I. Castor, C. Castro, W. Caughey, R. Cavitt, J. Celeste, P.M. Celliers, C. Cerjan, G. Chandler, B. Chang, C. Chang, J. Chang, L. Chang, R. Chapman, T.D. Chapman, L. Chase, H. Chen, H. Chen, K. Chen, L.-Y. Chen, B. Cheng, J. Chittenden, C. Choate, J. Chou, R.E. Chrien, M. Chrisp, K. Christensen, M. Christensen, N.S. Christiansen, A.R. Christopherson, M. Chung, J.A. Church, A. Clark, D.S. Clark, K. Clark, R. Clark, L. Claus, B. Cline, J.A. Cline, J.A. Cobble, K. Cochrane, B. Cohen, S. Cohen, M.R. Collette, G.W. Collins, L.A. Collins, T.J.B. Collins, A. Conder, B. Conrad, M. Conyers, A.W. Cook, D. Cook, R. Cook, J.C. Cooley, G. Cooper, T. Cope, S.R. Copeland, F. Coppari, J. Cortez, J. Cox, D.H. Crandall, J. Crane, R.S. Craxton, M. Cray, A. Crilly, J.W. Crippen, D. Cross, M. Cuneo, G. Cuotts, C.E. Czajka, D. Czechowicz, T. Daly, P. Danforth, C. Danly, R. Darbee, B. Darlington, P. Datte, L. Dauffy, G. Davalos, S. Davidovits, P. Davis, J. Davis, S. Dawson, R.D. Day, T.H. Day, M. Dayton, C. Deck, C. Decker, C. Deeney, K.A. DeFriend, G. Deis, N.D. Delamater, J.A. Delettrez, R. Demaret, S. Demos, S.M. Dempsey, R. Desjardin, T. Desjardins, M.P. Desjarlais, E.L. Dewald, J. DeYoreo, S. Diaz, G. Dimonte, T.R. Dittrich, L. Divol, S.N. Dixit, J. Dixon, A. Do, E.S. Dodd, D. Dolan, A. Donovan, M. Donovan, T. Döppner, C. Dorrer, N. Dorsano, M.R. Douglas, D. Dow, J. Downie, E. Downing, M. Dozieres, V. Draggoo, D. Drake, R.P. Drake, T. Drake, G. Dreifuerst, O. Drury, D.F. DuBois, P.F. DuBois, G. Dunham, M. Durocher, R. Dylla-Spears, A.K.L. Dymoke-Bradshaw, B. Dzenitis, C. Ebbers, M. Eckart, S. Eddinger, D. Eder, D. Edgell, M.J. Edwards, P. Efthimion, J.H. Eggert, B. Ehrlich, P. Ehrmann, S. Elhadj, C. Ellerbee, N.S. Elliott, C.L. Ellison, F. Elsner, M. Emerich, K. Engelhorn, T. England, E. English, P. Epperson, R. Epstein, G. Erbert, M.A. Erickson, D.J. Erskine, A. Erlandson, R.J. Espinosa, C. Estes, K.G. Estabrook, S. Evans, A. Fabyan, J. Fair, R. Fallejo, W.A.F. N. Farmer1, M. Farrell1, V. E. Fatherley5, M. Fedorov2, E. Feigenbaum2, T. Fehrenbach21, M. Feit2,a, B. Felker2, W. Ferguson2, J. C. Fernandez5, A. Fernandez-Panella2, S. Fess1, J. E. Field2, C. V. Filip2, J. R. Fincke5, T. Finn16, S. M.

Finnegan5, R. G. Finucane2, M. Fischer2, A. Fisher2, J. Fisher2, B. Fishler2, D. Fittinghoff2, P. Fitzsimmons1, M. Flegel2, K. A. Flippo5, J. Florio1, J. Folta2, P. Folta2, L. R. Foreman5,a, C. Forrest10, A. Forsman1, J. Fooks1, M. Foord2, R. Fortner2, K. Fournier2, D. E. Fratanduono2, N. Frazier16, T. Frazier2, C. Frederick1, M. S. Freeman5, J. Frenje3, D. Frey1, G. Frieders2, S. Friedrich2, D. H. Froula10, J. Fry2, T. Fuller1, J. Gaffney2, S. Gales22, B. Le Galloudec2, K. K. Le Galloudec2, A. Gambhir2, L. Gao14, W. J. Garbett22, A. Garcia1, C. Gates2, E. Gaut1, P. Gauthier15, Z. Gavin1, J. Gaylord2, C. G. R. Geddes12, M. Geissel7, F. Génin2, J. Georgeson7, H. Geppert-Kleinrath5, V. Geppert-Kleinrath5, N. Gharibyan2, J. Gibson1, C. Gibson1, E. Giraldez1, V. Glebov10, S. G. Glendinning2, S. Glenn2, S. H. Glenzer2,17, S. Goade1, P. L. Gobby5, S. R. Goldman5, B. Golick2, M. Gomez7, V. Goncharov10, D. Goodin1, P. Grabowski2, E. Grafil2, P. Graham22, J. Grandy2, E. Grasz2, F. R. Graziani2, G. Greenman, J. A. Greenough2, A. Greenwood1, G. Gregori23, T. Green2, J. R. Griego5, G. P. Grim2, J. Grondalski2, S. Gross13, J. Guckian9, N. Guler24, B. Gunney2, G. Guss2, S. Haan2, J. Hackbarth1, L. Hackel2, R. Hackel2, C. Haefner2,25,c, C. Hagmann2, K. D. Hahn2, S. Hahn2, B. J. Haid2, B. M. Haines5, B. M. Hall2, C. Hall7, G. N. Hall2, M. Hamamoto2, S. Hamel2, C. E. Hamilton5, B. A. Hammel2, J. H. Hammer2, G. Hampton2, A. Hamza2, A. Handler2, S. Hansen7, D. Hanson7, R. Haque2, D. Harding10, E. Harding7, J. D. Hares20, D. B. Harris5, J. A. Harte2, E. P. Hartouni2, R. Hatarik2, S. Hatchett2, A. A. Hauer5, M. Havre1, R. Hawley2, J. Hayes1, J. Hayes2,a, S. Hayes2, A. Hayes-Sterbenz5, C. A. Haynam2, D. A. Haynes5, D. Headley7, A. Heal2, J. E. Heebner2, S. Heerey2, G. M. Heestand2,a, R. Heeter2, N. Hein1, C. Heinbockel1, C. Hendricks2, M. Henesian2, J. Heninger2, J. Henrikson2, E. A. Henry2, E. B. Herbold2, M. R. Hermann2, G. Hermes2, J. E. Hernandez2, V. J. Hernandez2, M. C. Herrmann2, H. W. Herrmann5, O. D. Herrera2, D. Hewett2,a, R. Hibbard2, D. G. Hicks2,d, D. P. Higginson2, D. Hill1, K. Hill14, T. Hilsabeck2, D. E. Hinkel2, D. D. Ho2, V. K. Ho1, J. K. Hoffer5, N. M. Hoffman5, M. Hohenberger2, M. Hohensee2, W. Hoke1, D. Holdener2, F. Holdener2, J. P. Holder2, B. Holko1, D. Holunga2, J. F. Holzrichter2, J. Honig2, D. Hoover1, D. Hopkins2, L. F. Berzak Hopkins2, M. Hoppe, Jr.1, M. L. Hoppe, Sr.1, J. Horner2, R. Hornung2, C. J. Horsfield22, J. Horvath2, D. Hotaling2, R. House2, L. Howell2, W. W. Hsing2, S. X. Hu10, H. Huang1, J. Huckins2, H. Hui2, K. D. Humbird2, J. Hund1, J. Hunt2, O. A. Hurricane2, M. Hutton2, K. H.-K. Huynh2, L. Inandan1, C. Iglesias2, I. V. Igumenshchev10, I. Ivanovich26, N. Izumi2, M. Jackson1, J. Jackson2, S. D. Jacobs, G. James2, K. Jancaitis2, J. Jarboe2, L. C. Jarrott2, D. Jasion1, J. Jaquez1, J. Jeet2, A. E. Jenei2, J. Jensen1, J. Jimenez2, R. Jimenez1, D. Jobe16, Z. Johal1, H. M. Johns5, D. Johnson7, M. A. Johnson2, M. Gatu Johnson3, R. J. Johnson2, S. Johnson2, S. A. Johnson2, T. Johnson3, K. Jones7, O. Jones2,a, M. Jones7, R. Jorge1, H. J. Jorgenson5, M. Julian1, B. I. Jun2, R. Jungquist10, J. Kaae1, N. Kabadi3, D. Kaczala1, D. Kalantar2, K. Kangas1, V. V. Karasiev10, M. Karasik27, V. Karpenko2, A. Kasarky16, K. Kasper2, R. Kauffman2, M. I. Kaufman6, C. Keane2,e, L. Keaty1, L. Kegelmeyer2, P. A. Keiter5, P. A. Kellett20, J. Kellogg7, J. H. Kelly10, S. Kemic5, A. J. Kemp2, G. E. Kemp2, G. D. Kerbel2, D. Kershaw2, S. M. Kerr2, T. J. Kessler10, M. H. Key2, S. F. Khan2, H. Khater2, C. Kiikka2, J. Kilkenny1, Y. Kim5, Y.-J. Kim2, J. Kimko2, M. Kimmel7, J. M. Kindel16, J. King2, R. K. Kirkwood2, L. Klaus2, D. Klem2, J. L. Kline5, J. Klingmann2, G. Kluth15, P. Knapp7, J. Knauer10, J. Knipping1, M. Knudson7, D. Kobs1, J. Koch2,a, T. Kohut2, C. Kong1, J. M. Koning2, P. Koning2, S. Konior1, H. Kornblum2, L. B. Kot5, B. Kozioziemski2, M. Kozlowski2, P. M. Kozlowski5, J. Krammen2, N. S. Krasheninnikova5, C. M. Krauland1, B. Kraus14, W. Krauser5, J. D. Kress5, A. L. Kritcher2, E. Krieger2, J. J. Kroll2, W. L. Kruer2, M. K. G. Kruse2, S. Kucheyev2, M. Kumbera2, S. Kumpan2, J.

Kunimune3, E. Kur2, B. Kustowski2, T. J. T. Kwan5, G. A. Kyrala5, S. Laffite15, M. Lafon15, K. LaFortune17, L. Lagin2, B. Lahmann3,2, B. Lairson9, O. L. Landen2, T. Land2, M. Lane2, D. Laney2, A. B. Langdon2, J. Langenbrunner5, S. H. Langer2, A. Langro2, N. E. Lanier5, T. E. Lanier2, D. Larson2, B. F. Lasinski2, D. Lassle2, D. LaTray2, G. Lau2, N. Lau1, C. Laumann2, A. Laurence1, T. A. Laurence2, J. Lawson6, H. P. Le2, R. R. Leach2, L. Leal1, A. Leatherland22, K. LeChien2, B. Lechleiter2, A. Lee2, M. Lee1, T. Lee1, R. J. Leeper5, E. Lefebvre15, J.-P. Leidinger15, B. LeMire2, R. W. Lemke7, N. C. Lemos2, S. Le Pape2,28, R. Lerche2, S. Lerner2, S. Letts2, K. Levedahl16, T. Lewis2, C. K. Li3, H. Li2, J. Li2, W. Liao2, Z. M. Liao2, D. Liedahl2, J. Liebman2, G. Lindford2, E. L. Lindman5, J. D. Lindl2, H. Loey2, R. A. London2, F. Long7, E. N. Loomis5, F. E. Lopez5, H. Lopez9, E. Losbanos1, S. Loucks10, R. Lowe-Webb2, E. Lundgren1, A. P. Ludwigsen2, R. Luo1, J. Lusk2, R. Lyons2, T. Ma2, Y. Macallop13, M. J. MacDonald2, B. J. MacGowan2, J. M. Mack5, A. J. Mackinnon2, S. A. MacLaren2, A. G. MacPhee2, G. R. Magelssen5, J. Magoon10, R. M. Malone6, T. Malsbury2, R. Managan2, R. Mancini29, K. Manes2, D. Maney2,a, D. Manha2, O. M. Mannion7, A. M. Manuel2, M. J.-E. Manuel1, E. Mapoles2, G. Mara2, T. Marcotte1, E. Marin1, M. M. Marinak2, D. A. Mariscal2, E. F. Mariscal2, E. V. Marley2, J. A. Marozas10, R. Marquez1, C. D. Marshall2, F. J. Marshall10, M. Marshall10, S. Marshall16, J. Marticorena2, J. I. Martinez5, D. Martinez2, I. Maslennikov2, D. Mason2, R. J. Mason5, L. Masse2,15, W. Massey2, P.-E. Masson-Laborde15,30, N. D. Masters2, D. Mathisen2, E. Mathison1, J. Matone2, M. J. Matthews2, C. Mattoon2, T. R. Mattsson7, K. Matzen7, C. W. Mauche2, M. Mauldin1, T. McAbee2, M. McBurney2, T. Mccarville2, R. L. McCrory, Jr.10, A. M. McEvoy5, C. McGuffey1, M. Mcinnis1, P. McKenty10, M. S. McKinley2, J. B. McLeod2, A. McPherson7, B. Mcquillan1,a, M. Meamber2, K. D. Meaney5, N. B. Meezan2, R. Meissner2, T. A. Mehlhorn7, N. C. Mehta2, J. Menapace2, F. E. Merrill5, B. T. Merritt2, E. C. Merritt5, D. D. Meyerhofer5, S. Mezyk2, R. J. Mich2, P. A. Michel2, D. Milam2, C. Miller2, D. Miller2, D. S. Miller2, E. Miller2, E. K. Miller6, J. Miller2,a, M. Miller2, P. E. Miller2, T. Miller1, W. Miller1, V. Miller-Kamm2, M. Millot2, J. L. Milovich2, P. Minner2, J.-L. Miquel15, S. Mitchell2, K. Molvig5, R. C. Montesanti2, D. S. Montgomery5, M. Monticelli2, A. Montoya7, J. D. Moody2, A. S. Moore2, E. Moore2, M. Moran2, J. C. Moreno2, K. Moreno1, B. E. Morgan2, T. Morrow5, J. W. Morton22, E. Moses2, K. Moy6, R. Muir2, M. S. Murillo31,32, J. E. Murray2, J. R. Murray2,a, D. H. Munro2, T. J. Murphy5, F. M. Munteanu2, J. Nafziger1, T. Nagayama7, S. R. Nagel2, R. Nast1, R. A. Negres2, A. Nelson7, D. Nelson10, J. Nelson2, S. Nelson16, S. Nemethy2, P. Neumayer2,f, K. Newman2, M. Newton2, H. Nguyen2, J.-M. G. Di Nicola2, P. Di Nicola2, C. Niemann2,33, A. Nikroo2, P. M. Nilson10, A. Nobile5, V. Noorai1, R. C. Nora2, M. Norton2, M. Nostrand2, V. Note2, S. Novell2, P. F. Nowak2, A. Nunez1, R. A. Nyholm2, M. O'Brien2, A. Oceguera2, J. A. Oertel5, A. L. Oesterle34, J. Okui2, B. Olejniczak2, J. Oliveira2, P. Olsen2, B. Olson2, K. Olson2, R. E. Olson5, Y. P. Opachich2, N. Orsi2, C. D. Orth2, M. Owen2, S. Padalino2,35, E. Padilla2, R. Paguio1, S. Paguio1, J. Paisner5, S. Pajoom1, A. Pak2, S. Palaniyappan5, K. Palma2, T. Pannell2, F. Papp2, D. Paras1, T. Parham2, H.-S. Park2, A. Pasternak13, S. Patankar2, M. V. Patel2, P. K. Patel2,b, R. Patterson2, S. Patterson2, B. Paul9, M. Paul2, E. Pauli2, O. T. Pearce2, J. Pearcy3, A. Pedretti2, B. Pedrotti2, A. Peer2, L. J. Pelz2, B. Penetrante2,a, J. Penner2, A. Perez1, L. J. Perkins2, E. Pernice2, T. S. Perry5, S. Person2, D. Petersen2, T. Petersen2, D. L. Peterson5,a, E. B. Peterson1, J. E. Peterson2, J. L. Peterson2, K. Peterson7, R. R. Peterson5, R. D. Petrasso3, F. Philippe15, D. Phillion2, T. J. Phipps1, E. Piceno1, L. Pickworth2,g, Y. Ping2, J. Pino2, K. Piston2, R. Plummer2, G. D. Pollack5, S. M. Pollaine2, B. B. Pollock2, D. Ponce1, J. Ponce1, J. Pontelandolfo1, J. L. Porter7, J. Post2, O.

Poujade15,30, C. Powell2, H. Powell2,a, G. Power2, M. Pozulp2, M. Prantil2, M. Prasad2, S. Pratuch2, S. Price1, K. Primdahl2, S. Prisbrey2, R. Procassini2, A. Pruyne10, B. Pudliner2, S. R. Qiu2, K. Quan1, M. Quinn1, J. Quintenz1, P. B. Radha10, F. Rainer2, J. E. Ralph2, K. S. Raman2, R. Raman2, P. W. Rambo2, S. Rana2, A. Randewich22, D. Rardin2, M. Ratledge1, N. Ravelo1, F. Ravizza2, M. Rayce2, A. Raymond1, B. Raymond2, B. Reed2, C. Reed1, S. Regan10, B. Reichelt3, V. Reis16, S. Reisdorf2, V. Rekow2, B. A. Remington2, A. Rendon2, W. Requieron1, M. Rever2, H. Reynolds1, J. Reynolds1, J. Rhodes2, M. Rhodes2, M. C. Richardson10,h, B. Rice10, N. G. Rice1, R. Rieben2, A. Rigatti10, S. Riggs2, H. G. Rinderknecht10, K. Ring1, B. Riordan1, R. Riquier15, C. Rivers1, D. Roberts2, V. Roberts2, G. Robertson7, H. F. Robey5, J. Robles1, P. Rocha2, G. Rochau7, J. Rodriguez1, S. Rodriguez2, M. D. Rosen2, M. Rosenberg10, G. Ross2, J. S. Ross2, P. Ross16, J. Rouse2, D. Rovang7, A. M. Rubenchik2,a, M. S. Rubery2, C. L. Ruiz7, M. Rushford2, B. Russ1, J. R. Rygg10, B. S. Ryujin2, R. A. Sacks2, R. F. Sacks5, K. Saito1, T. Salmon2, J. D. Salmonson2, J. Sanchez2, S. Samuelson16, M. Sanchez7, C. Sangster10, A. Saroyan2, J. Sater2, A. Satsangi16, S. Sauers2, R. Saunders2, J. P. Sauppe5, R. Sawicki2, D. Sayre2, M. Scanlan2, K. Schaffers2, G. T. Schappert5, S. Schiaffino2,a, D. J. Schlossberg2, D. W. Schmidt5, P. F. Schmit2, J. M. Smidt5, D. H. G. Schneider2, M. B. Schneider2, R. Schneider16, M. Schoff1, M. Schollmeier7, C. R. Schroeder2, S. E. Schrauth2, H. A. Scott2, I. Scott1, J. M. Scott5, R. H. H. Scott36, C. R. Scullard2, T. Sedillo5, F. H. Seguin3, W. Seka10, J. Senecal2, S. M. Sepke2, L. Seppala2, K. Sequoia1, J. Severyn2, J. M. Sevier2, N. Sewell2, S. Seznec15, R. C. Shah10, J. Shamlian10, D. Shaughnessy2, M. Shaw2, R. Shaw2, C. Shearer1, R. Shelton2, N. Shen2, M. W. Sherlock2, A. I. Shestakov2, E. L. Shi2, S. J. Shin2, N. Shingleton2, W. Shmayda10, M. Shor2, M. Shoup10, C. Shuldberg1, L. Siegel2, F. J. Silva1, A. N. Simakov5, B. T. Sims16, D. Sinars7, P. Singh1, H. Sio3,2, K. Skulina2, S. Skupsky10, S. Slutz7, M. Sluyter16,a, V. A. Smalyuk2, D. Smauley2, R. M. Smeltser7, C. Smith2, I. Smith7, J. Smith1, L. Smith2, R. Smith2, R. Smith9, M. Schölmerich2, R. Sohn1, S. Sommer2, C. Sorce10, M. Sorem5, J. M. Soures10, M. L. Spaeth2, B. K. Spears2, S. Speas7, D. Speck2, R. Speck2, J. Spears2, T. Spinka2, P. T. Springer2, M. Stadermann2, B. Stahl1, J. Stahoviak7, J. Stanley2, L. G. Stanton2,37, R. Steele2, W. Steele2,a, D. Steinman1,a, R. Stemke1, R. Stephens1, S. Sterbenz6, P. Sterne2, D. Stevens2, J. Stevers2, C. H. Still2,a, C. Stoeckl10, W. Stoeffl2, J. S. Stolken2, C. Stolz2, E. Storm2, G. Stone2, S. Stoupin2, E. Stout2, I. Stowers2, R. Strauser1, H. Streckart1, J. Streit13, D. J. Strozzi2, J. Stutz1, L. Summers2, T. Suratwala2, G. Sutcliffe3, L. J. Suter2, S. B. Sutton2, V. Svidzinski2, G. Swadling2, W. Sweet1, A. Szoke2,a, M. Tabak2, M. Takagi2, A. Tambazidis1, V. Tang2, M. Taranowski2, L. A. Taylor2, S. Telford2, W. Theobald10, M. Thi1, A. Thomas2, C. A. Thomas2,10, I. Thomas2,a, R. Thomas7,a, I. J. Thompson2, A. Thongstisubskul1, C. B. Thorsness2, G. Tietbohl2, R. E. Tipton2, M. Tobin2, N. Tomlin1, R. Tommasini2, A. J. Toreja2, J. Torres7, R. P. J. Town2, S. Townsend2, J. Trenholme2,a, A. Trivelpiece2, C. Trosseille2, H. Truax1, D. Trummer2, S. Trummer2, T. Truong16, D. Tubbs5, E. R. Tubman2, T. Tunnell6, D. Turnbull10, R. E. Turner2, M. Ulitsky2, R. Upadhye2, J. L. Vaher2, P. VanArsdall2, D. VanBlarcom2, M. Vandenboomgaerde15, R. VanQuinlan2, B. M. Van Wonterghem2, W. S. Varnum5, A. L. Velikovich27, A. Vella2, C. P. Verdon16, B. Vermillion1, S. Vernon2, R. Vesey7, J. Vickers1, R. M. Vignes2, M. Visosky16, J. Vocke1, P. L. Volegov5, S. Vonhof1, R. Von Rotz2, H. X. Vu5, M. Vu1, D. Wall1, J. Wall1, R. Wallace2, B. Wallin2, D. Walmer2, C. A. Walsh2, C. F. Walters2, C. Waltz2, A. Wan2, A. Wang2, Y. Wang2, J. S. Wark23, B. E. Warner2, J. Watson2, R. G. Watt5, P. Watts2, J. Weaver27, R. P. Weaver5, S. Weaver2, C. R. Weber2, P. Weber2, S. V. Weber2, P. Wegner2, B. Welday2, L. Welser-Sherrill5, K. Weiss2,

K. B. Wharton38, G. F. Wheeler2, W. Whistler2,a, R. K. White2, H. D. Whitley2, P. Whitman2, M. E. Wickett2, K. Widmann2, C. Widmayer2, J. Wiedwald2, R. Wilcox12, S. Wilcox2, C. Wild21, B. H. Wilde5, C. H. Wilde5, K. Wilhelmsen2, M. D. Wilke5,a, H. Wilkens1, P. Wilkins2, S. C. Wilks2, E. A. Williams2, G. J. Williams2, W. Williams2, W. H. Williams2, D. C. Wilson5, B. Wilson2, E. Wilson2, R. Wilson2, S. Winters2, P. J. Wisoff2, M. Wittman10, J. Wolfe2, A. Wong2, K. W. Wong2, L. Wong2, N. Wong2, R. Wood2, D. Woodhouse1, J. Woodruff2,a, D. T. Woods2, S. Woods1, B. N. Woodworth2, E. Wooten1, A. Wootton2, K. Work6, J. B. Workman5, J. Wright2, M. Wu7, C. Wuest6, F. J. Wysocki5, H. Xu1, M. Yamaguchi1, B. Yang2, S. T. Yang2, J. Yatabe2, C. B. Yeamans2, B. C. Yee2, S. A. Yi5, L. Yin5, B. Young2, C. S. Young5, C. V. Young2, P. Young2, K. Youngblood1, J. Yu2, R. Zacharias2, G. Zagaris2, N. Zaitseva2, F. Zaka2, F. Ze2, B. Zeiger9, M. Zika2, G. B. Zimmerman2, T. Zobrist2, J. D. Zuegel10, and A. B. Zylstra2,i Achievement of Target Gain Larger than Unity in an Inertial Fusion Experiment, Phys. Rev. Lett., 132 (2024) 065102.
[15] J. Biener, T. Braun, T. Lee, W.L. York, M. Nielsen, W. Sun, C. Aracne-Ruddle, S.M. Hayes, M.M. Biener, L.B. Bayu Aji, T. Fehrenbach, C. Wild, R.K. Rai, E.A. Stach, W. Nieveen, Understanding Macroscopic and Microscopic properties of Tungsten Doped Nanocrystalline Diamond Coatings that Enabled Ignition at the National Ignition Facility, to be submitted to Nature Materials, DOI (2024).
[16] R. Nora, R. Betti, K.S. Anderson, A. Shvydky, A. Bose, K.M. Woo, A.R. Christopherson, J.A. Marozas, T.J.B. Collins, P.B. Radha, S.X. Hu, R. Epstein, F.J. Marshall, R.L. McCrory, T.C. Sangster, D.D. Meyerhofer, Theory of hydro-equivalent ignition for inertial fusion and its applications to OMEGA and the National Ignition Facility, Physics of Plasmas, 21 (2014) 056316.

FIGURE CAPTIONS

Figure 1 Illustration of the frustraum utilized at the NIF, comprising two conical frustum-shaped hohlraums conjoined along the capsule's equator.

Figure 2 a) Down-scattered ratio divided by the initial ice thickness versus coast time. b) Down-scattered ratio divided by the initial ice thickness versus coast time, adjusted for yield amplification, mode 1, and mode 2 corrections. Bubble size reflects the tungsten areal density in the capsules for each implosion.

Figure 3 Comparison of laser pulse shapes between a HyE keyhole (N211031) and the frustraum 780 keyhole (N220608) is illustrated by the solid black and red lines, respectively. The dashed black (N211031) and dashed red (N220608) lines represent the unfolded shock velocity in liquid deuterium for these experiments.

Figure 4 The measured hotspot shapes from the frustraum 780 campaign are depicted, showing the x-ray image from the 2D-ConA N220523 in Fig. 4a and the neutron image from the symcap N220627 in Fig. 4b.

Figure 5 X-ray images captured through the laser entrance holes (LEH) at 6 ns, showing the bubble motion with varying levels of quad splitting on the 50° cones. Fig. 5a represents no quad splitting, while Fig. 5b and Fig. 5c illustrate quad splittings of $\pm$275 μm and $\pm$400 μm, respectively, within a given 50° quad.

Figure 6 Comparison of laser pulse shapes between a HyE keyhole, N211031, and the frustraum 820 keyhole, N221005, depicted as solid black and red lines, respectively. The unfolded shock velocity in the liquid deuterium for these two experiments is indicated by the dashed black (N211031) and dashed red (N221005) lines.

Figure 7 Measured hotspot shapes from the frustraum 820 campaign, displaying the neutron image from the symcap N221113 in Fig. 7a and the x-ray image from the 2D-ConA N221220 in Fig. 7b.

Figure 8 a) Radiograph of the imploding hotspot on the 2D-ConA experiment N221220 showing an x-pattern in the data. b) Drawing of the 2D-ConA platform depicting two 50° quads driving a backlighter foil used to radiograph the capsule in flight. c) Drawing of the existing 2D-ConA target with a square diagnostic cutout and window. d) Proposed 2D-ConA target with a circular diagnostic cutout and window.

Figure 9 Plot showing the hotspot shapes and the level of hotspot P2 as a function of the frustraum wall angle for several of the initial 1100 frustraum experiments.

Figure 10 Symmetry plot of the x-ray P2 shape in experiments conducted in the Frustraum platform through calendar year 2022. These experiments include four different capsule inner radii (1050, 1100, 1200, and 1400 μm), three wall angles (21, 23, and 25 degrees), and five frustraum equatorial diameters (7, 7.8, 8.2, 9.26, and 9.75 mm). The bubble size is proportional to the inner radius of the ablator capsule to the 5th power.

Figure 11 Peak Dante Flux as a function of effective laser energy (Adding 6.5% for Au-lined DU). The frustraum experiments (7.8 mm diameter in red and 8.2 mm diameter in green) above 1.2 MJ (symcaps and 2D-ConAs) are shown as red diamonds and green triangles, respectively. All of the

HyE shots with a 3.1 mm LEH (DTs, THDs, symcaps, and 2D-ConAs) are shown as blue circles. The ratio of the fits suggests a 14% increase in the peak Dante Flux to the 7/8 power as a function of laser energy into the hohlraum for the 8.2 mm frustraum experiments relative to HyE

Figure 12 Plot of the implosion acceleration time versus effective laser energy into the hohlraums.

Figure 13 Plot showing the ion temperature driven in symcaps and 2D-ConAs as a function of effective laser energy.

Figure A1 Plot showing the simulated DSR degradation (black circles) due to mode 1. The dashed red line represents a fit of (1-(DDSR/DSR/2)^2) to the degradation. The dashed blue line represents the fit of (1-1.6*(DDSR/DSR/2)^2.7) to the degradation.

Table 1 Comparison of capsules used in the IRaum experiment N211009, the HyE experiment N221204, and the capsule built for layered implosions in the frustraum 820 platform.

Table 2 Summary of 1-D capsule-only simulations comparing the HyE shot N221204 with a simulated layered implosion in the frustraum 820 platform.

FIGURES

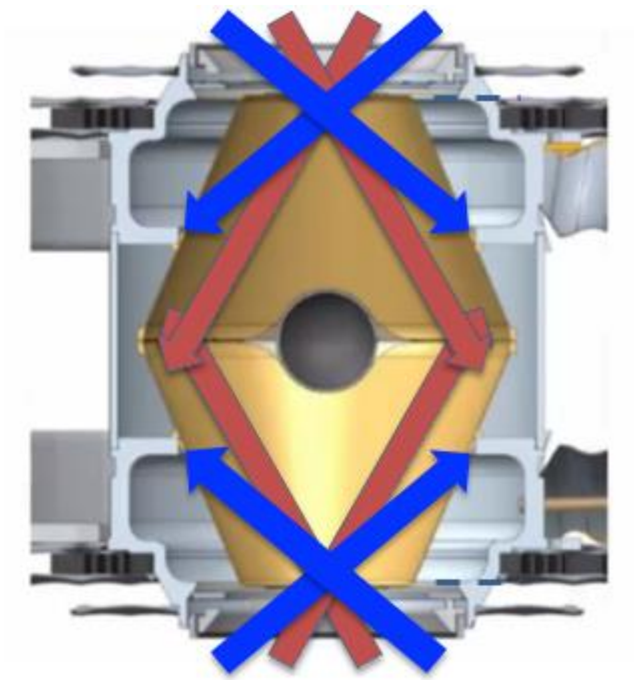

Figure 1

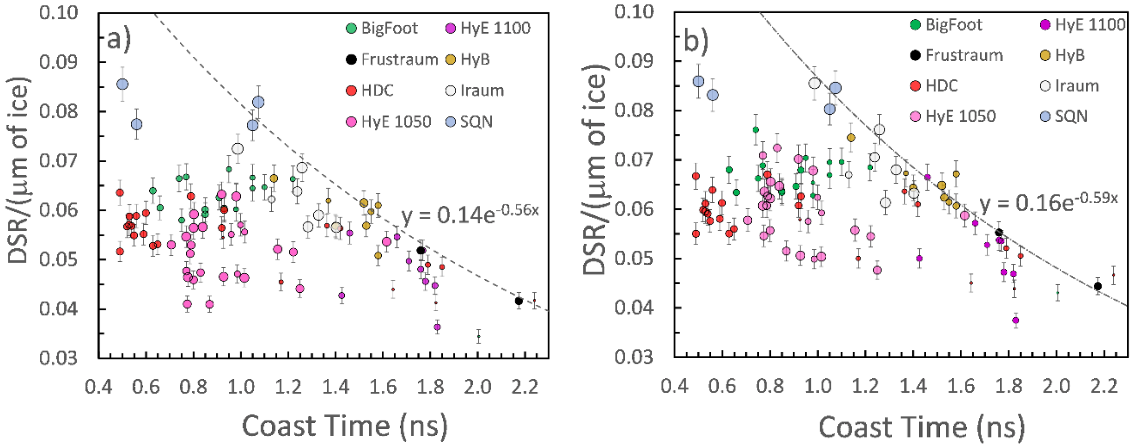
a)
b)
DSR/(µm of ice)
Coast Time (ns)
BigFoot
HyE 1100
Frustraum
HyB
HDC
Iraum
HyE 1050
SQN
y = 0.14e^-0.56x
y = 0.16e^-0.59x
0.10
0.09
0.08
0.07
0.06
0.05
0.04
0.03
0.4
0.6
0.8
1.0
1.2
1.4
1.6
1.8
2.0
2.2

Figure 2

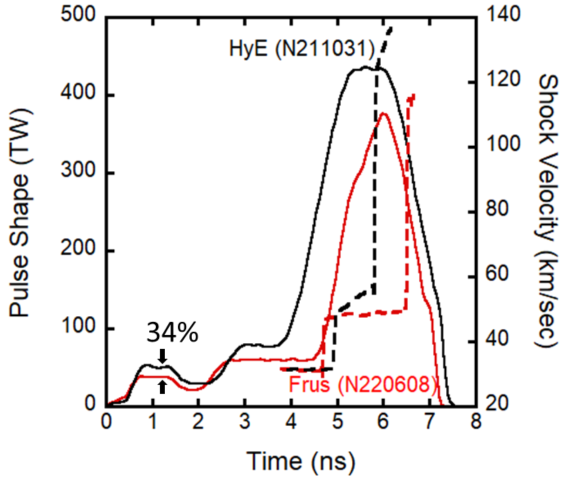

Pulse Shape (TW)
Shock Velocity (km/sec)
Time (ns)
HyE (N211031)
Frus (N220608)
34%
500
400
300
200
100
0
140
120
100
80
60
40
20
0
1
2
3
4
5
6
7
8

Figure 3

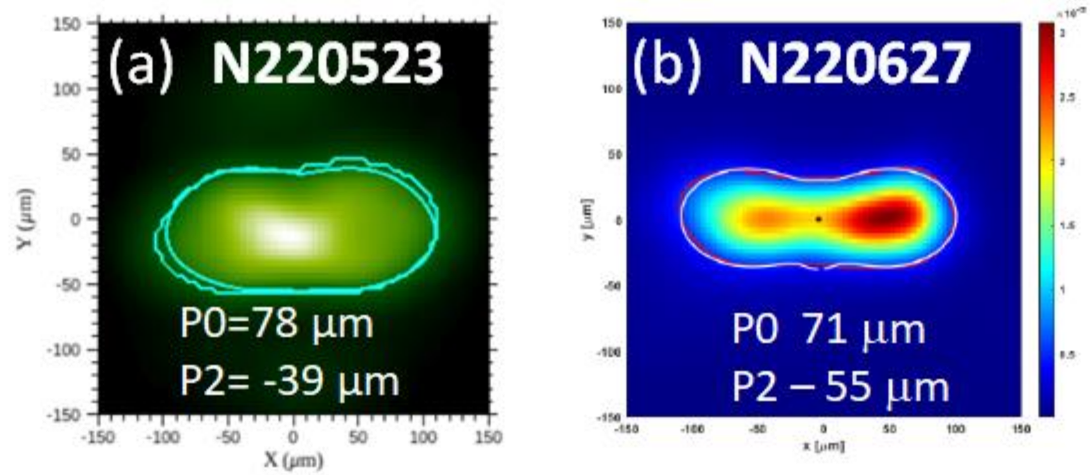
(a) N220523
P0=78 µm
P2= -39 µm
Y (µm)
X (µm)
(b) N220627
P0 71 µm
P2 – 55 µm
y [µm]
x [µm]

Figure 4

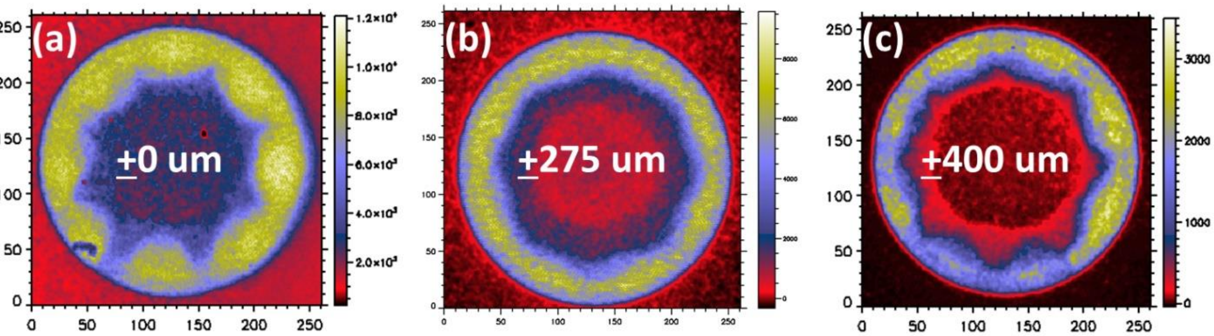

Figure 5

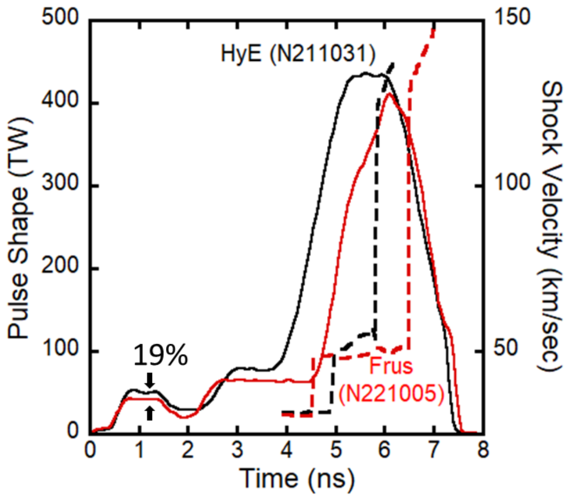

HyE (N211031)
19%
Frus
(N221005)
Pulse Shape (TW)
Shock Velocity (km/sec)
Time (ns)
0
100
200
300
400
500
50
100
150
0
1
2
3
4
5
6
7
8

Figure 6

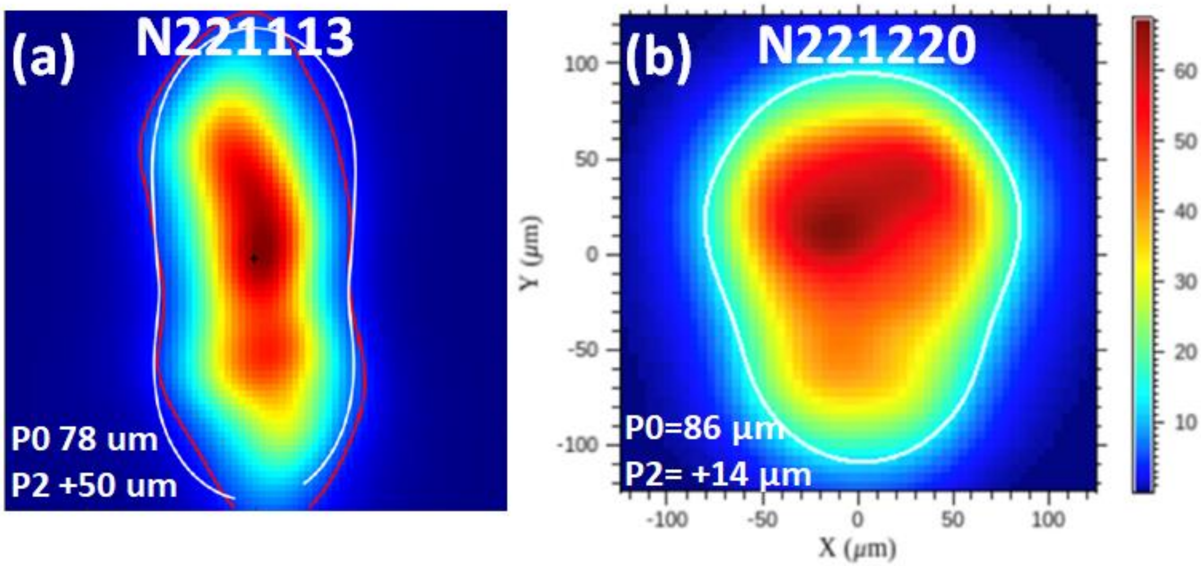
(a)
N221113
P0 78 um
P2 +50 um
(b)
N221220
P0=86 µm
P2= +14 µm
Y (µm)
X (µm)
100
50
0
-50
-100
-100
-50
0
50
100
60
50
40
30
20
10

Figure 7

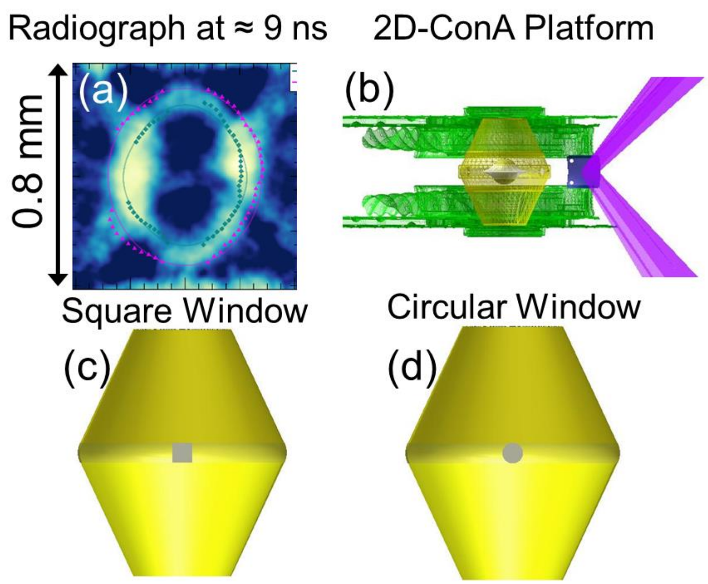
Radiograph at ≈ 9 ns
2D-ConA Platform
(a)
0.8 mm
(b)
Square Window
Circular Window
(c)
(d)

Figure 8

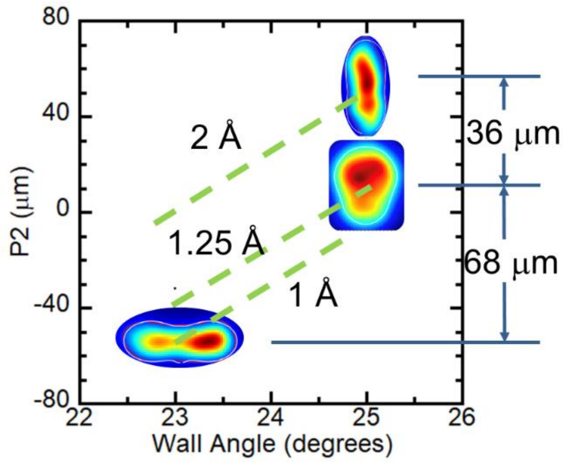
80
40
0
-40
-80
22
23
24
25
26
P2 (μm)
Wall Angle (degrees)
2 Å
1.25 Å
1 Å
36 μm
68 μm

Figure 9

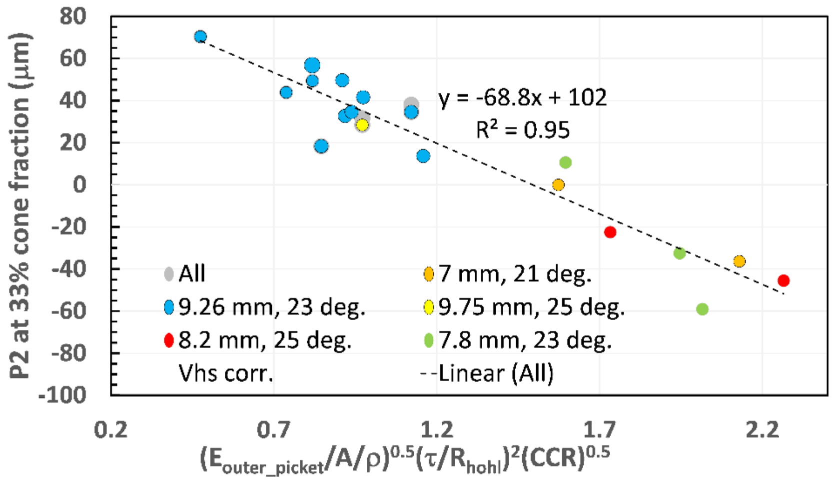
80
60
40
20
0
-20
-40
-60
-80
-100
P2 at 33% cone fraction (μm)
y = -68.8x + 102
R² = 0.95
All
9.26 mm, 23 deg.
8.2 mm, 25 deg.
Vhs corr.
7 mm, 21 deg.
9.75 mm, 25 deg.
7.8 mm, 23 deg.
Linear (All)
0.2
0.7
1.2
1.7
2.2
(E_outer_picket/A/ρ)^0.5(τ/R_hohl)^2(CCR)^0.5

Figure 10

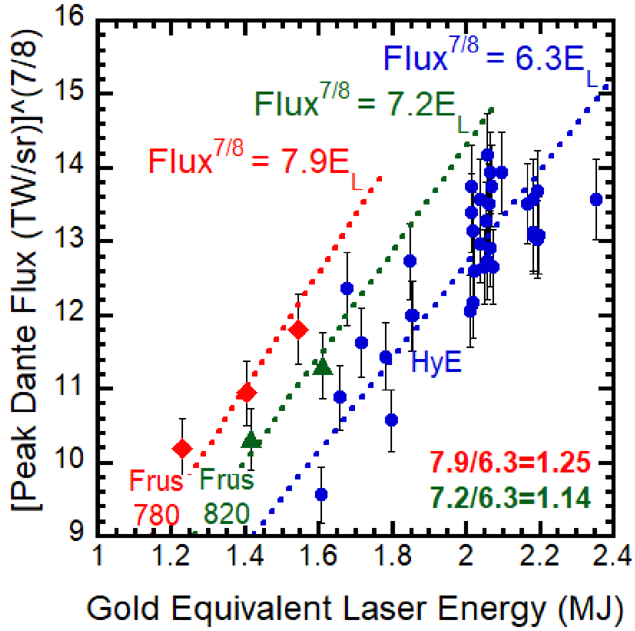
Flux7/8 = 6.3EL
Flux7/8 = 7.2EL
Flux7/8 = 7.9EL
HyE
7.9/6.3=1.25
7.2/6.3=1.14
Frus 780
Frus 820
[Peak Dante Flux (TW/sr)]^(7/8)
Gold Equivalent Laser Energy (MJ)
16
15
14
13
12
11
10
9
1
1.2
1.4
1.6
1.8
2
2.2
2.4

Figure 11

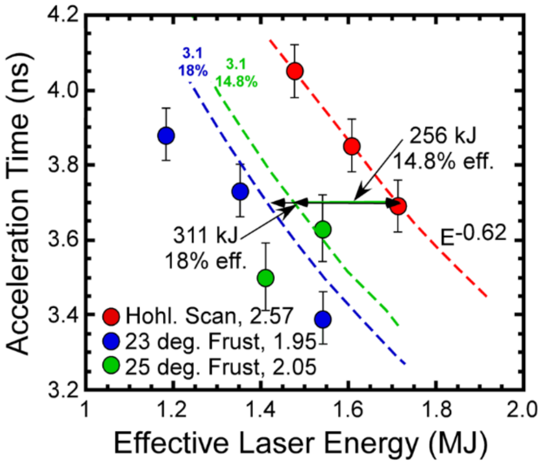

Acceleration Time (ns)
Effective Laser Energy (MJ)
3.1
18%
3.1
14.8%
256 kJ
14.8% eff.
311 kJ
18% eff.
E-0.62
Hohl. Scan, 2.57
23 deg. Frust, 1.95
25 deg. Frust, 2.05

Figure 12

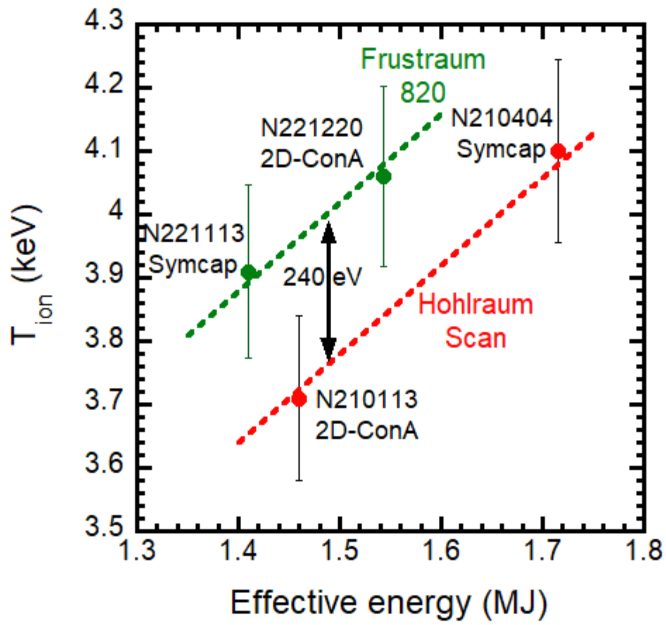

Frustraum
820
N221220
2D-ConA
N210404
Symcap
N221113
Symcap
240 eV
Hohlraum
Scan
N210113
2D-ConA
T ion (keV)
Effective energy (MJ)
4.3
4.2
4.1
4
3.9
3.8
3.7
3.6
3.5
1.3
1.4
1.5
1.6
1.7
1.8

Figure 13

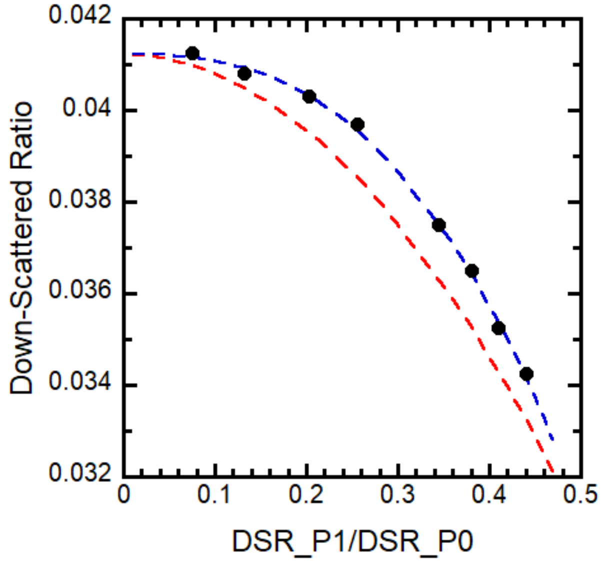
0.042
0.04
0.038
0.036
0.034
0.032
Down-Scattered Ratio
0
0.1
0.2
0.3
0.4
0.5
DSR_P1/DSR_P0

Figure A1

	N211009 KC826	N221204 KC952	Frustraum DT KC1116	Scaling
Capsule inner radius (mm)	1	1.05	1.1	S
Layer 1 mass (mg)	0.211	0.236	0.267	S^3
Layer 1 thick. (μm)	4.99	5.07	6.05	S
Layer 2 mass (mg)	1.004	0.790	1.299	S^3
Layer 2 thick. (μm)	22.9	16.239	23.6	S
Layer 2 W (%)	0.53	0.61	0.47	S^{-2}
Layer 2 W rR (μm %)	12.14	9.91	11.1	S^{-1}
Layer 3 mass (mg)	2.354	3.223	3.25	S^3
Layer 3 thick. (μm)	50.41	63.05	57.38	S
Total Mass (mg)	3.68	4.249	4.81	S^3
Total thick. (μm)	80.57	84.36	87.45	S

Table 1

1-D simulations with preheat	N221204 HyE KC952	Frustraum Kc1116	Percent Difference
Cap. I.R.	1.05 mm	1.1 mm	+5%
Laser Energy	2.05 MJ	1.85 MJ	-10%
Abs. Energy (kJ)	243	280	+15%
Yield 1D (MJ)	14.1	18.1	+28%
ρR (g/cm^3) no α	1.4	1.5	+7%
DSR (%) no α	5.3	5.6	+6%
T_{ion} (keV) no α	4.6	5	+9%
P_{hs} (Gbar) no α	280	310	+11%
E_{hs} (kJ) no α	10.4	11.3	+9%
GLP(PE$^{0.5}$) no α	1.6	1.9	+19%

Table 2